Atmos. Chem. Phys. Discuss., 12, 12801–12852, 2012
www.atmos-chem-phys-discuss.net/12/12801/2012/
doi:10.5194/acpd-12-12801-2012

Atmospheric Chemistry and Physics Discussions

In-canopy gas-phase chemistry during CABINEX 2009: sensitivity of a 1-D canopy model to vertical mixing and isoprene chemistry

A. M. Bryan[1], S. B. Bertman[2], M. A. Carroll[1], S. Dusanter[3,4,5], G. D. Edwards[6], R. Forkel[7], S. Griffith[8], A. B. Guenther[9], R. F. Hansen[8], D. Helmig[10], B. T. Jobson[11], F. N. Keutsch[12], B. L. Lefer[13], S. N. Pressley[11], P. B. Shepson[14,15], P. S. Stevens[8], and A. L. Steiner[1]

[1]Department of Atmospheric, Oceanic, and Space Sciences, University of Michigan, Ann Arbor, Michigan, 48109, USA
[2]Department of Chemistry, Western Michigan University, Kalamazoo, Michigan, 49008, USA
[3]School of Public and Environmental Affairs, Indiana Univ., Bloomington, Indiana, 47405, USA
[4]EMDouai, CE, 59508 Douai, France
[5]Univ Lille Nord de France, 59000, Lille, France
[6]Department of Chemistry, Eastern Michigan University, Ypsilanti, Michigan, 48197, USA
[7]Karlsruhe Institute of Technology (KIT), IMK-IFU, 82467 Garmisch-Partenkirchen, Germany
[8]Department of Chemistry, Indiana University, Bloomington, Indiana, 47405, USA

[9]Atmospheric Chemistry Division, National Center for Atmospheric Research, Boulder, Colorado, 80307, USA
[10]Institute of Arctic and Alpine Research, Univ. of Colorado, Boulder, Colorado, 80309, USA
[11]Department of Civil & Environmental Engineering, Washington State University, Pullman, Washington, 99164, USA
[12]Department of Chemistry, University of Wisconsin, Madison, Wisconsin, 53706, USA
[13]Department of Earth and Atmospheric Sciences, University of Houston, Houston, Texas, 77004, USA
[14]Department of Chemistry, Purdue University, West Lafayette, Indiana, 47907, USA
[15]Department of Earth and Atmospheric Sciences, Purdue University, West Lafayette, Indiana, 47907, USA

Received: 22 February 2012 – Accepted: 7 May 2012 – Published: 22 May 2012

Correspondence to: A. M. Bryan (ambrya@umich.edu)

Published by Copernicus Publications on behalf of the European Geosciences Union.

ACPD
12, 12801–12852, 2012

Abstract

Vegetation emits large quantities of biogenic volatile organic compounds (BVOC). At remote sites, these compounds are the dominant precursors to ozone and secondary organic aerosol (SOA) production, yet current field studies show that atmospheric models have difficulty in capturing the observed HO_x cycle and concentrations of BVOC oxidation products. In this manuscript, we simulate BVOC chemistry within a forest canopy using a one-dimensional canopy-chemistry model (Canopy Atmospheric CHemistry Emission model; CACHE) for a mixed deciduous forest in northern Michigan during the CABINEX 2009 campaign. We find that the base-case model, using fully-parameterized mixing and the simplified biogenic chemistry of the Regional Atmospheric Chemistry Model (RACM), underestimates daytime in-canopy vertical mixing by 50–70 % and by an order of magnitude at night, leading to discrepancies in the diurnal evolution of HO_x, BVOC, and BVOC oxidation products. Implementing observed micrometeorological data from above and within the canopy substantially improves the diurnal cycle of modeled BVOC, particularly at the end of the day, and also improves the observation-model agreement for some BVOC oxidation products and OH reactivity. We compare the RACM mechanism to a version that includes the Mainz isoprene mechanism (RACM-MIM) to test the model sensitivity to enhanced isoprene degradation. RACM-MIM simulates higher concentrations of both primary BVOC (isoprene and monoterpenes) and oxidation products (HCHO, MACR + MVK) compared with RACM simulations. Additionally, the revised mechanism alters the OH concentrations and increases HO_2. These changes generally improve agreement with HO_x observations yet overestimate BVOC oxidation products, indicating that this isoprene mechanism does not improve the representation of local chemistry at the site. Overall, the revised mechanism yields smaller changes in BVOC and BVOC oxidation product concentrations and gradients than improving the parameterization of vertical mixing with observations, suggesting that uncertainties in vertical mixing parameterizations are an important component in understanding observed BVOC chemistry.

ACPD

12, 12801–12852, 2012

1 Introduction

There is increasing evidence of the important role of forest canopies and biogenic volatile organic compound (VOC) emissions on tropospheric composition and atmospheric chemistry (Goldstein and Galbally, 2007; Lelieveld et al., 2008). VOC oxidation, in the presence of reactive nitrogen oxides ($NO_x = NO + NO_2$) and sunlight, is critical for ozone formation (Logan, 1985) and condensation of their oxidation products can yield secondary organic aerosols (SOA) (Claeys et al., 2004; Carlton et al., 2009; Hallquist et al., 2009). Additionally, VOC can control the oxidation capacity of the troposphere through the regulation of hydrogen radicals ($HO_x = OH + HO_2$) chemistry (Poisson et al., 2000; Tan et al., 2001). Forest canopies are an important VOC source both globally and regionally, contributing to nearly half the global VOC budget (Guenther et al., 1995). To affect the troposphere, biogenic VOC (BVOC) emissions and their oxidation products must be mixed effectively out of the forest canopy. This forest-atmosphere exchange is highly sensitive to turbulent mixing and chemistry because BVOC oxidation and transport occur on similar timescales (Molemaker and Vilà-Guerau de Arellano, 1998; Krol et al., 2000; Pugh et al., 2010).

To investigate the role of BVOC on tropospheric chemistry, several recent field campaigns have involved chemical measurements at multiple heights throughout the forest canopy (e.g., Carroll et al., 2001; Hewitt et al., 2010; Martin et al., 2010). Results from these field campaigns highlight gaps in our understanding of BVOC oxidation. For example, the hydroxyl radical (OH) is underestimated in most forest ecosystem types (Carslaw and Carslaw, 2001; Tan et al., 2001; Butler et al., 2008; Karl et al., 2009). Modeling studies of remote forest sites that add a HO_x recycling mechanism through BVOC oxidation reactions (Lelieveld et al., 2008; Hofzumahaus et al., 2009) or OH regeneration from epoxides (Paulot et al., 2009) display some improvement in measured-modeled agreement in some locations, yet these do not show consistent improvement in all studies (Karl et al., 2009; Barkley et al., 2011). Additionally, BVOC oxidation products are poorly simulated in a number of forest regimes. Pugh et al. (2010) show that

ACPD
12, 12801–12852, 2012

first-generation oxidation products of isoprene (C_5H_8, 2-methyl-1,3-butadiene) – the dominant BVOC emission in many broadleaf ecosystems – are overestimated by box-model simulations of a Malaysian tropical rainforest. Karl et al. (2009) compare several mechanisms with enhanced isoprene oxidation and find that some isoprene oxidation products such as hydroxyacetone are underpredicted compared to observations. While revised chemical mechanisms can explicitly account for more detailed isoprene chemistry (Pöschl et al., 2000; Paulot et al., 2009; Peeters et al., 2009; Stavrakou et al., 2010), difficulties remain in simulating isoprene degradation and oxidation products under low-NO_x conditions (Karl et al., 2009).

In addition to uncertainties in the pathways of BVOC oxidation, vertical transport within and above the canopy sub-layer is an additional source of uncertainty in forest-atmosphere exchange (Finnigan, 2000; Hurst et al., 2001). Here, we define the canopy sub-layer as the thin atmospheric layer nearest the surface containing forest roughness elements. Turbulence in the planetary boundary layer (PBL) occurs at sub-grid scales in most atmospheric models and, thus, must be parameterized. Among the most common parameterizations is the first-order flux-gradient relationship, known as K-theory, in which turbulent exchange is a function of the eddy diffusivity parameter, K (Blackadar, 1979). Because mixing strength in the mid-PBL peaks at two orders of magnitude higher than near the canopy roughness layer (Gao et al., 1993), turbulent transport tends to be much smaller within plant canopies than above the roughness elements. In fact, K-theory has been found to break down completely within forest canopies due to the existence of intermittent coherent structures (Raupach et al., 1996), yet the parameterization continues to be used for its computational efficiency in many models (Forkel et al., 2006). Though high-resolution canopy models may have the vertical resolution to capture fine-scale turbulence within the canopy, many models do not have the detailed description of higher-order turbulence to simulate the effects of coherent structures and other canopy-scale turbulence. Near-field effects, often represented by a scaling factor (Makar et al., 1999; Stroud et al., 2005; Wolfe and Thornton, 2011), have been shown to improve modeled in-canopy and above-canopy turbulence (Raupach, 1989).

ACPD
12, 12801–12852, 2012

Large-eddy simulation models (e.g., Heus et al., 2010; Patton et al., 2001) can capture these dynamical changes, but are typically coupled to chemical mechanisms that are insufficiently detailed to accurately capture the features needed to trace isoprene and its oxidation products. Therefore, most models have large uncertainties in the role of vertical mixing on BVOC gradients and forest-atmosphere exchange (e.g., Ganzeveld et al., 2006).

Despite the uncertainties in vertical mixing, one-dimensional (1-D) models are still useful tools for studying the vertical transport in the context of atmospheric composition because they can focus on the implications of in-canopy chemistry on vertical concentrations and gradients within a forest canopy (e.g., Wolfe et al., 2011; Boy et al., 2011). Wolfe et al. (2011) conclude that chemistry may outweigh the effect of turbulent mixing on forest-atmosphere exchange, even for compounds with long chemical lifetimes relative to their transport timescales. However, the authors limit their focus to in-canopy chemistry without consideration for mixing parameterizations and uncertainty. In addition, their simulations are limited to midday at a single point in time, and BVOC emissions from their environment of study are predominantly monoterpenes, with low levels of isoprene emissions. Boy et al. (2011) applies a more detailed turbulence scheme to understand BVOC oxidation and tracer transport and their effect on particle formation in a Scots Pine forest in Finland. They find that this improved mixing parameterization can reproduce observed vertical profiles of BVOC.

Here, we focus on chemistry and turbulence within and above a deciduous hardwood forest in Northern Michigan. A number of field campaigns as part of the Program for Research on Oxidants: PHotochemistry, Emissions, and Transport (PROPHET, Carroll et al., 2001) have been conducted since 1997 at the University of Michigan Biological Station (UMBS). Results from the summer 1998 PROPHET intensive show that models underestimate OH (Faloona et al., 2001; Sillman et al., 2002), while measured HO_2 concentrations compare well with model results (Tan et al., 2001). Measurements of OH reactivity suggest an unknown potential BVOC source, which may contribute to these OH discrepancies (Di Carlo et al., 2004). In 2009, the Community

ACPD
12, 12801–12852, 2012

Atmosphere-Biosphere INteractions Experiment (CABINEX) was conducted to provide new insights into the role of BVOC chemistry and its relationship to HO_x chemistry observed at the PROPHET site. Branch enclosure measurements from CABINEX 2009 show that identified primary emissions reasonably reflect current emission estimates (Ortega et al., 2007), suggesting that the missing ambient OH reactivity could be explained by secondary oxidation (Kim et al., 2011).

In this manuscript, we compare measurements from the CABINEX 2009 campaign with a 1-D Eulerian Canopy Atmospheric CHemistry Emission model (CACHE, Forkel et al., 2006) to investigate the role of in-canopy chemistry and turbulence on HO_x and BVOC concentrations and vertical gradients. To examine the relative sensitivities of the model to mixing and chemistry, we compare a base-case model scenario with the original turbulence and chemistry description within CACHE against a revised mixing scheme and isoprene-focused chemical mechanism. We explore the relative impacts of HO_x pathways in an atmospheric chemical mechanism versus the effects of vertical mixing on ambient concentrations to isolate and highlight the key processes of biosphere-atmosphere interactions at this deciduous forest ecosystem.

2 Methods

2.1 Site and data description

CABINEX 2009 was conducted at the PROPHET site at UMBS near Pellston, MI (45°33′31.66″ N, 84°43′52.40″ W) at the transition between mixed hardwood to boreal forest (Schmid et al., 2003). Depending on the wind direction, the site can be controlled by local emissions and chemistry or regional transport from urban areas (Milwaukee, WI (∼ 378 km SW); Detroit, MI (∼ 385 km SSE); and Chicago, IL (∼ 475 km SW), as shown in Supplement Fig. S1). The local vegetation is diverse (Pressley et al., 2005), containing varieties of aspen, oak, beech, birch, maple, and pine with an average canopy height (h) of approximately 22.5 m. Climate conditions at the PROPHET

ACPD
12, 12801–12852, 2012

site are generally cold but with warm summers (FLUXNET database, Baldocchi et al., 2001). The average daily maximum temperatures for Pellston, MI, in July and August are 26 °C and 25 °C with average precipitation of 63.2 mm and 81.8 mm, respectively. The summer of 2009 was unseasonably cool and cloudy with an average high temperature of 22 °C and with rain or fog occurring on 62 % of the days within the 1 July–8 August 2009 observational period, which has implications for reduced BVOC emissions and photochemistry.

CABINEX measurements of O_3, NO_2, NO, isoprene, monoterpenes, formaldehyde (HCHO), methacrolein and methyl vinyl ketone (MACR + MVK), OH, HO_2, and glyoxal (GLY) were conducted at multiple heights within and above the canopy. Due to limited instrumentation during the campaign, simultaneous measurements at multiple heights could not be obtained for all compounds. Therefore, data availability at a given height widely varies over the campaign. Primary BVOC species and BVOC oxidation products were measured, alternating at 10-min intervals between 6 m, 20.4 m, and 34 m, using a proton transfer reaction mass spectrometer (PTR-MS) with dehumidified sampling to allow more sensitive measurement of HCHO (de Gouw and Warneke, 2007; Jobson and McCoskey, 2010). NO and NO_2 were measured, alternating between the same three heights, using a 2-channel chemiluminescence instrument with a blue light photolytic converter for NO_2 (Air Quality Design). HO_x species were measured only at 32 m during the two-day simulation presented here, with OH measured using laser-induced fluorescence with the Fluorescence Assay by Gas Expansion (FAGE) technique and HO_2 measured by chemical conversion to OH with added NO (Stevens et al., 1994; Dusanter et al., 2009). Total OH reactivity was measured at 30.9 m using a turbulent flow tube technique similar to that described in Kovacs and Brune (2001). Glyoxal (GLY) was measured at 35.4 m using laser-induced phosphorescence (Huisman et al., 2011). Wind speed and direction were measured via propeller anemometer at 36.4 m. Additionally, two sonic anemometers measuring the three-component wind field (u, v, and w) and temperature were mounted at 20.6 m and 34 m (Steiner et al., 2011). Temperature was also measured at 6 m, 20.4 m, and 31.2 m using R. M. Young relative humidity

ACPD
12, 12801–12852, 2012

and temperature probes. Photosynthetically active radiation (PAR) was measured at 32.6 m using a BF-3 Sunshine Sensor.

2.2 Model description

CACHE is a 1-D multilayer model that simulates the vertical distribution of concentrations and vertical fluxes of heat, moisture, and gas-phase chemical species over time using the prognostic equations for temperature (T) and mass (c):

$$\frac{\partial T}{\partial t} = \frac{\partial}{\partial z}\left(K_{\mathrm{H}}\frac{\partial T}{\partial z}\right) + S_{\mathrm{H}} \quad (1)$$

$$\frac{\partial c}{\partial t} = \frac{\partial}{\partial z}\left(K_{\mathrm{H}}\frac{\partial c}{\partial z}\right) + S_{\mathrm{c}} + C \quad (2)$$

Equations (1) and (2) are solved for each model layer, where K_{H} denotes the turbulent exchange coefficient for heat, S_{h} and S_{c} denote sources and sinks for heat and mass, respectively, and C denotes chemical transformation. The model domain consists of 40 layers spanning 4.4 km in the vertical (z) direction. In our simulations, we include eight layers within the 6-m trunk vertical column and ten layers in the 16.5-m vertical crown space. The grid resolution decreases exponentially with height with a spacing of 0.81 m at ground level and 1061.1 m at the top. Simulations are run for 48 h at a time step of 60 s. Model output is interpolated at the instrument heights and data collection times for precise comparison with measurements. Turbulent exchange, chemistry, and advection, as treated in CACHE, are described in subsequent sections, along with a discussion of the site-specific model setup and description of the BVOC and soil NO emission parameterizations. Full description of the remaining model components are presented in Forkel et al. (2006).

ACPD
12, 12801–12852, 2012

2.2.1 Turbulent exchange

In its original configuration, vertical transport is parameterized in CACHE using a first-order flux-gradient relationship, or K-theory, in which heat and mass are transported by eddy diffusion at a rate proportional to the turbulent exchange coefficient, K_H. Vertical fluxes of heat and mass are computed at each model time step as follows:

$$\overline{w'\theta'} = -K_H \frac{\partial \bar{\theta}}{\partial z} \tag{3}$$

$$\overline{w'c'} = -K_H \frac{\partial \bar{c}}{\partial z} \tag{4}$$

K_H is derived empirically according to Forkel et al. (1990) given a length scale l, a vertical wind shear $|\partial V_g/\partial z|$, and a stability parameter f based on the Richardson number (Ri):

$$K_H = l^2 \left| \frac{\partial V_g}{\partial z} \right| \cdot f(Ri) \tag{5}$$

To evaluate the sensitivity of BVOC gradients to in-canopy vertical mixing, we apply a modified K-theory parameterization following Makar et al. (1999). K_H in Eqs. (1) and (2) is derived from the friction velocity (u^*) and vertical velocity standard deviation (σ_w), and the near-field effects of the canopy on turbulence are considered. In this alternate scheme (hereafter referred to as the "MIX" simulation), we adjust the modeled K_H profile with derived measurements of u^* and σ_w at 20.6 m (0.92 h) and 34 m (1.51 h) according to the expression:

$$K_H = \sigma_w^2 T_L \tag{6}$$

ACPD
12, 12801–12852, 2012

where T_L is the Lagrangian timescale ($T_L = 0.3\,h/u^*$). u^* and σ_w are computed using half-hour Reynolds averages of raw (10 Hz) sonic anemometer measurements of u, v, and w:

$$u^* = \left(\overline{u'w'}^2 + \overline{v'w'}^2\right) \tag{7}$$

$$\sigma_w = \sqrt{\frac{1}{n-1}\sum_{i=1}^{n}(w_i - \bar{w})^2} \tag{8}$$

Half-hour averaging filters out small-scale intermittent coherent structures (i.e., sweeps and ejections, as observed by Collineau and Brunet, 1993; Finnigan, 2000) that may be important for releasing plumes of biogenic emissions out of the canopy (Butler et al., 2008; Pugh et al., 2010); consequently, BVOC segregation, induced by coherent structures and other non-Fickian diffusive processes, is not captured in our model. At each time step, a K_H profile is initially calculated according to Forkel et al. (1990) using the modeled vertical profiles of temperature and wind speed. Then, we linearly interpolate K_H between the canopy base (6 m) and the first measurement level (20.6 m) following Eq. (6). Next, we adjust modeled K_H from the first (20.6 m) to the second measurement level (34 m) using linear interpolations of u^* and σ_w measurements. Near-canopy K_H ($z \leq 1.64\,h$) is scaled by an R factor to account for near-field effects of the canopy, where R is:

$$R = \frac{\left[1 - \exp\left(-\tau/T_L\right)\right](\tau - T_L)^{3/2}}{\left[\tau - T_L + T_L \exp\left(-\tau/T_L\right)\right]^{3/2}} \tag{9}$$

and the transport timescale τ is derived using a τ/T_L ratio of 4 (Stroud et al., 2005; Wolfe and Thornton, 2011). Above 34 m, modeled values are adjusted to remove any

ACPD
12, 12801–12852, 2012

discontinuity between the measured and modeled values, and midday values peak at approximately 500 m with a maximum mixing height of 1 km. We evaluate the revised mixing scheme in Sect. 3.1.

2.2.2 Chemistry

Gas-phase chemical transformation in the original CACHE model implements the Regional Atmospheric Chemistry Mechanism (RACM, Stockwell et al., 1997), which includes a suite of 77 chemical species and 237 reactions. The mechanism includes explicit treatment of three BVOC categories: isoprene (denoted by the RACM surrogate, ISO), monoterpenes with one double bond (i.e., α-pinene; denoted API), and monoterpenes with two double bonds (i.e., *d*-limonene; denoted LIM). The remaining VOC are lumped into four alkane categories, four alkene categories, and three aromatic categories based on reactivity with OH. In the RACM mechanism, MACR + MVK are contained in the surrogate for all unsaturated C4 carbonyls (denoted MACR in Stockwell et al., 1997), which derive from both anthropogenic and biogenic diene oxidation; however, we note that measurements from the campaign only account for MACR + MVK alone.

In this study, we perform a sensitivity test (hereafter referred to as the "MIM" simulation) comparing RACM against the Mainz isoprene mechanism (MIM) adaptation of RACM (RACM-MIM, Geiger et al., 2003). RACM-MIM treats an additional seven species explicitly that are split from surrogate species in RACM. By using this greater speciation, RACM-MIM includes an additional twelve reactions. Ultimately, this mechanism provides more specific pathways of isoprene oxidation, the production of second-generation isoprene oxidation products, and further detail on the MACR chemistry under low-NO_x conditions.

ACPD
12, 12801–12852, 2012

2.2.3 Advection

Horizontal advection of anthropogenic NO_x and long-lived VOC is represented in CACHE as a function of wind direction. Cooper et al. (2001) attribute elevated concentrations of O_3, CO, NO_x, and other oxidized nitrogen species (NO_z) observed at PROPHET to southerly flow from Chicago or Detroit and lower mixing ratios to flow from clean Canadian air masses over the Great Lakes. We estimate the direction-dependent advection rate of eight RACM species (NO_2, HCHO, MACR, KET, HC3, HC5, OLT, and OLI; see Stockwell et al. (1997) for full definitions) according to the geographical location of PROPHET relative to nearby major urban centers. Chicago (pop. ∼ 2.9 million) and Detroit (pop. ∼950 000) are the major contributors of anthropogenic emissions affecting northern Michigan, with emission inventories for NO_x and VOC totaling over 20 000 kg day^{-1}, whereas peak NO_x and VOC emissions from Milwaukee (pop. ∼950 000) total in the range of 12 500–15 000 kg day^{-1} (LADCO, 2010). Therefore, we presume signatures of anthropogenic advection observed at PROPHET to be more pronounced with air originating in Chicago or Detroit over Milwaukee by assuming the strongest advection rates when winds are directly from the south. Westerly advection from Lake Michigan has been associated with lower isoprene concentrations than advection from forests to the south (Sillman et al., 2002); therefore, we add advection of biogenic HCHO and MACR from isoprene oxidation under southerly winds. We incorporate advection of the above species between the heights 45–106 m (22–26 model levels) at the hourly, wind-direction-dependent rates shown in Table 1. Measured NO_2, HCHO, and MACR concentrations are used to tune advection rates for the model scenario that incorporates both nudged turbulence and RACM-MIM chemistry (hereafter, the MIX + MIM case). Due to the lack of ambient observations, anthropogenic hydrocarbon RACM categories, OLI, OLT, KET, HC3, and HC5, are added to reflect average concentrations of regional pollution events.

ACPD
12, 12801–12852, 2012

2.3 Case study description and model setup

The case study simulation period includes 48 h starting at 00:00 Eastern Standard Time (EST) on 4 August 2009 and ending at 23:59 EST on 5 August 2009. This two-day period offers the clearest daytime skies within the period when the most chemistry observations are available. We select these clear-sky days because they represent the time period most conducive to BVOC emissions and photochemistry, as well as providing the best measured-modeled agreement for the turbulence parameterization. NCEP surface reanalysis indicates a weak frontal passage occurring at ~07:00 EST on 4 August (Fig. S1), visible in the observed wind direction (Fig. S2) through a shift from southerly to northwesterly winds. Back-trajectory data (Fig. S1) show that air originated in northern Illinois (southwest of the PROPHET site) prior to the frontal passage. Following the frontal passage, the source region ranges from northern Minnesota and southwestern Ontario, Canada (west and northwest of the site, respectively). This meteorological scenario allows us to evaluate our advection scheme presented in Sect. 2.2.3 and the ability of the model to capture the shift from polluted- to clean-air advection, while also providing a good comparison between chemistry at PROPHET under the influence of regional transport versus predominantly local chemistry.

We adapt CACHE for the PROPHET site by adjusting site-specific parameters, including the total leaf area index (LAI) (3.8 $m^2\,m^{-2}$, Ortega et al., 2007) and the leaf reflectance and transmittance (values for a typical deciduous broadleaf ecosystem used in this study are shown in Table 2, Asner, 1998). Initial conditions are provided to the model for vertical profiles of chemical concentrations based on observed above-canopy concentrations at 00:00 EST on 4 August 2009; the initial vertical temperature profile is interpolated using radiosonde data from Gaylord, MI (~ 59.5 km S). Model input includes (Fig. S2): (1) observed PAR to drive the prognostic temperature profile and photochemistry and account for cloud cover, and (2) observed wind speed and direction at 36.4 m to drive the vertical wind profile and NO_x and VOC advection; additional

ACPD
12, 12801–12852, 2012

input required for the revised turbulence scheme (the MIX scenario, see Sect. 2.2.1) include u^* and σ_w at 20.6 and 34 m. Above the canopy, winds are scaled according to the logarithmic-wind equation (Stull, 1988); within the canopy, winds dissipate as a function of u^* and a canopy structure according to a modified logarithmic-wind equation following Baldocchi (1988).

BVOC emissions are controlled by site-specific emission rates that depend on ecosystem-specific emission factors, temperature, and PAR (Steinbrecher et al., 1999). Isoprene emission fluxes were not routinely measured during the campaign; therefore, we use the mean isoprene surface emission flux observed at PROPHET during 2003 and 2005 (Ortega et al., 2007). Big tooth aspen (*Populus grandidentata*) and red oak (*Quercus rubra*) account for 99 % of the isoprene budget, emitting at mean basal emission rates of 46.3 and 53.5 $\mu g C g^{-1} h^{-1}$ at standard conditions (PAR = 1000 $\mu mol m^{-2} s^{-1}$; temperature = 30 °C). Since 2009 was colder than average summers, we subtract one standard deviation from the mean isoprene emission fluxes, corresponding to 24.8 $\mu g C g^{-1} h^{-1}$ for aspen and 23.8 $\mu g C g^{-1} h^{-1}$ for oak. The net emission of isoprene per model level is determined by scaling the given emission factors by PAR and temperature, according to the parameterization described in Forkel et al. (2006) following Guenther et al. (1995), and a prescribed vertical LAI distribution. Monoterpene emission rates derive from tree branch enclosure measurements in the 2003, 2005 and 2009 (Ortega et al., 2007; Ortega and Helmig, 2008). Normalized (20 °C) foliage emission rates for the sum of monoterpenes for red oak (*Quercus rubra*), white pine (*Pinus strobus*), red pine (*Pinus resinosa*), and American beech (*Fagus grandifolia*) measured during CABINEX 2009 are 0.16, 0.38, 0.56, and 7.46 $\mu g C g^{-1} h^{-1}$, respectively. For beech, the predominant emission is *d*-limonene (27 %), followed by sabinene (17 %), α-pinene (12 %), and cymene (12 %). Ortega et al. (2007) measure a mean basal emission rate for paper birch (*Betula papyrifera*) of 0.5 $\mu g C g^{-1} h^{-1}$. For white and red pine, we scale the emission factors by 2.56 (Perterer and Körner, 1990) to account for the conversion from projected to total leaf area. We sum these species contributions and split this total monoterpene emission factor into

ACPD
12, 12801–12852, 2012

the RACM species API (56.5 %, or 0.086 nmol m^{-2} leaf area s^{-1}) and LIM (43.5 %, or 0.066 nmol m^{-2} leaf area s^{-1}) according to the measured fractional contribution of similar species.

We note that these emission estimates are based on available data from the site collected by several investigators over several seasons. Due to the high variability seen in these data, it is difficult to define representative values particularly given the cool conditions during the summer of 2009. Previous studies have noted that emission factors can vary based on prior temperatures on the span of weeks (Pétron et al., 2001) and can vary based on the plants acclimation, particularly for isoprene (Hanson and Sharkey, 2001). Consequently, these estimates may have uncertainties of a minimum of a factor of two. Measurements indicate a dependence on temperature for monoterpene emissions; therefore, we presume monoterpene emissions to be from pools within the foliage, and are, thus, scaled according to the temperature-dependent parameterization described in Forkel et al. (2006). Soil NO emissions are parameterized according to Forkel et al. (2006), following Simpson et al. (1995), based on an emission rate of 180 nmol m^{-2} h^{-1} observed previously at PROPHET (Alaghmand et al., 2011).

3 Results and discussion

We compare micrometeorological and chemistry observations from CABINEX 2009 against CACHE simulations during the 4–5 August 2009 case period using four model scenarios: (1) a base-case control run using fully-parameterized mixing according to Forkel et al. (1990) and RACM chemistry (hereafter referred to as the "BASE" scenario); (2) adjusted mixing according to Makar et al. (1999), as described in Sect. 2.2.1, also with RACM chemistry (hereafter, "MIX"); (3) fully-parameterized (i.e., BASE) mixing with RACM-MIM chemistry (hereafter, "MIM"); and (4) a combination of adjusted mixing by Makar et al. (1999) and RACM-MIM chemistry ("MIX + MIM"). We first evaluate the modifications made to the turbulent exchange parameterization implemented in the MIX model scenario (Sect. 3.1), followed by an analysis of model-measurement

ACPD
12, 12801–12852, 2012

comparisons throughout the canopy and the surface layer (to approximately 3 h) for O_3 and NO_x (Sect. 3.2), BVOC and their oxidation products (Sect. 3.3), and HO_x concentrations and OH reactivity (Sect. 3.4).

3.1 Evaluation of turbulent exchange

To test the sensitivity of BVOC gradients to in-canopy mixing, we perform simulations with CACHE using the two vertical mixing schemes presented in Sect. 2.2.1. Figure 1 compares the observed and modeled (BASE) eddy diffusivity (K_H) for the 4–5 August case study in the upper canopy (20.6 m, 0.92 h) and above the canopy (34 m, 1.92 h). At 34 m, measured K_H ranges from 3 $m^2 s^{-1}$ at night to 10 $m^2 s^{-1}$ at midday with nighttime and daytime standard deviations of around 1 and 2 $m^2 s^{-1}$, respectively. Upper-canopy measurements are only 1–3 $m^2 s^{-1}$ lower than above the canopy, with a similar magnitude of standard deviations. The majority of the canopy foliage resides below the 0.92 h measurement, and the absence of lower canopy micrometeorological measurements is a limiting factor in our estimates of in-canopy mixing. Modeled BASE K_H is below one standard deviation of the measurements at both measurement heights 95 % of the time during the BASE simulation. At 1.51 h, daytime BASE modeled values are underestimated by a factor of two, whereas nighttime values are two orders of magnitude below observations. Observed K_H at 0.92 h are an order of magnitude greater than model estimations over the full simulation period. In addition, the modeled diurnal pattern shows a decrease in mixing earlier in the day than observed, which is attributed to the lack of buoyancy-driven mixing in the modeled K_H. In Eq. (5), the Richardson number reduces mixing significantly under stable conditions. Because the BASE model parameterization typically classifies stable conditions when PAR decreases at the end of the day, the modeled K_H abruptly decreases at the onset of sunset resulting in an end-of-day decrease in mixing that is nearly two hours earlier than observed. We note that CACHE does not account for heat storage within the canopy biomass and this is also likely contributing to the early onset of stability in the model at the end of the day.

ACPD
12, 12801–12852, 2012

We evaluate the MIX turbulence scheme by comparing the BASE and MIX model simulations against observed midday vertical profiles of K_H, temperature, primary BVOC (isoprene and monoterpenes), and BVOC oxidation products (formaldehyde, MACR + MVK, and acetaldehyde) (Fig. 2). Observed values of K_H, which drive in-canopy turbulence profile for the MIX case, are twice as large as the BASE-case turbulence at 1.51 h and an order of magnitude larger at 0.92 h (Fig. 2a), indicating missing turbulence (e.g., coherent structures or counter-gradient terms) in the original K-theory parameterization. The standard deviations of the measurements (denoted by the error bars) are based on daily averages for the sunny and partly sunny days during the period of available u^* and σ_w measurements (21, 29 July, 2, 4, 5, and 7 August). Of these "clear-sky" days, observed turbulence was stronger than average on 5 Aug, leading to nearly uniform temperatures with height that is well captured by the MIX model case (Fig. 2b). In the BASE scenario, K_H decreases to 0.1 $m^2 s^{-1}$ at the displacement height, creating an unrealistic artificial boundary. This is an artifact of the use of two different equations to construct the in- and above-canopy wind profiles and turbulence schemes, which creates a discontinuity at the forest-atmosphere interface and prevents BVOC transport out of the canopy sub-layer in the model. Temperature (Fig. 2b) decreases with height within and above the canopy according to the observations, yet the BASE model case imposes a stabilizing inversion induced by heating of the upper canopy. Consequently, in-canopy mixing is weak in the BASE simulation. Observed midday vertical gradients of BVOC and oxidation products are also compared against the BASE and MIX simulations in Fig. 2b–2g. Enhanced turbulence effectively improves the agreement of modeled and measured concentrations for the more reactive species (isoprene and monoterpenes) by reducing in-canopy concentrations and weakening the vertical gradient. For the longer-lived species (formaldehyde, MACR + MVK, and acetaldehyde), concentrations are decreased and gradients are weakened by the enhanced mixing, leading to a nearly uniform modeled vertical profile in the lowest 60 m (3 h). Despite these improvements, the vertical transport in and above the canopy is still limited due to missing coherent structures and other sources of non-Fickian diffusion.

ACPD
12, 12801–12852, 2012

3.2 O_3 and NO_x

Figure 3 shows measurements of O_3, NO_2, and NO at the three measurement heights at the PROPHET tower versus the BASE, MIX, MIM, and MIX + MIM model scenarios during the 4–5 August simulation period. At all three heights, observed O_3 mixing ratios peak at 40–50 ppbv shortly after midnight at the beginning of the first day of simulation. Based on the synoptic conditions and wind trajectories (Fig. S1), this elevated O_3 is from advective transport rather than local production, which is supported by a concurrent NO_2 peak. Following the frontal passage discussed in Sect. 2.3, observed O_3 drops by 20 ppbv over 5 h as winds shift from southerly to northwesterly, marking the change from polluted- to clean-air advection. Following the 4-August peak, O_3 mixing ratios remain approximately constant at 30 ppbv above the canopy with some variability observed within the canopy. The model simulates a strong diurnal cycle for the BASE and MIM cases, with lower concentrations at night and higher concentrations during the day than observed at 34 and 20.4 m. Increasing the mixing (MIX scenario) dampens the O_3 diurnal cycles, which compares well with the 34 and 20.4 m observations. The midday maximum deposition velocity of O_3 is 1.6 $cm\,s^{-1}$, which is higher than other modeling studies rates of 0.4 $cm\,s^{-1}$ (Finkelstein et al., 2000; Stroud et al., 2005). Midday ozone deposition velocity increases by less than 0.1 $cm\,s^{-1}$ with enhanced mixing, suggesting the lack of diurnal cycle is driven by the changes in mixing. At 6 m, O_3 concentrations simulated by the MIX case are higher than observed, and all model versions have difficulty in capturing the changes in the diurnal cycle of ozone. This suggests that in-canopy O_3 concentrations are more influenced by local chemistry than regional transport at the canopy-scale, as observed, e.g., by Wolfe et al. (2011).

Like O_3, observed NO_2 displays a signature of anthropogenic advection on the early morning of 4 August. In the model, we have tuned the NO_2 advection rate (Sect. 2.2.3) to capture the higher concentrations observed at the beginning of the simulation and subsequent lower concentrations as the winds shift following the frontal passage. Observed NO_2 ranges from 1.2 ppbv at the beginning of the simulation to approximately

ACPD
12, 12801–12852, 2012

0.5 ppbv on the second night, with midday concentrations of less than 0.1 ppbv after photolysis. MIX + MIM underpredicts NO_2 slightly in the early part of the second night, likely due to an oversimplification in our NO_2 advection scheme or a missing NO_2 source in the model. NO mixing ratios show a distinct diurnal pattern in the observations, peaking at nearly 180 pptv around mid-morning 5 August at 34 m, consistent with measurements taken over multiple years at PROPHET (Alaghmand et al., 2011). At night, mixing ratios reach as low as 1–5 pptv. The model reproduces the NO diurnal cycle well at the top of the canopy in all model scenarios, with concentrations overestimated on the first day in the BASE and MIM cases and good agreement for the MIX cases, and underestimated on the second day in the MIX and MIX + MIM cases. NO concentrations decrease with increasing canopy depth as a result of light attenuation lowering the NO yields from NO_2 photolysis. All four model scenarios are able to capture this effect of attenuation reasonably well.

3.3 Biogenic VOC and oxidation products

Figure 4 evaluates the four model scenarios against observations for primary BVOC, isoprene and monoterpenes. Observations of isoprene show a strong diurnal cycle ranging from 0.2 ppbv at night to up to 2–3 ppbv at midday at all height levels. MIM simulations show slightly increased concentrations of isoprene over the BASE simulation, owing to lower OH availability as enhanced MACR + MVK concentrations increase the competition for OH. However, the BASE and MIM model scenarios have difficulty reproducing this diurnal pattern in two respects: (1) modeled concentrations increase later in the morning than observed, and (2) a rapid increase in concentrations occurs at sunset, causing a large discrepancy between the model and observations. Near the ground, this modeled pattern is dampened with a less pronounced evening peak and better drawdown of concentrations at night. Such a pattern has been long-observed (cf. Martin et al., 1991), and the modeled diurnal pattern is prevalent in many modeling studies (e.g., Sillman et al., 2002; Forkel et al., 2006; Barkley et al., 2011), which attribute the end-of-the-day increase to subsidence associated with the compression

ACPD
12, 12801–12852, 2012

of the PBL. CACHE does not incorporate an explicit dynamic boundary layer height, yet this feature is still prevalent in modeled isoprene concentrations at sunset. However, as demonstrated in the MIX simulation, enhanced turbulence dampens the sunset isoprene increase. The evening isoprene increase in the BASE case is concurrent with the transition from buoyancy-driven to mechanically-driven turbulence, when K_H decreases rapidly as stable conditions reduce vertical mixing (modeled as a function of the Richardson number; see Eq. 5). The sunset feature in the BASE isoprene concentrations exists because the sharp decrease in buoyancy-driven mixing leads to an equalization of above and below-canopy mixing, thereby increasing isoprene concentrations within and above the canopy. Additionally, weak in-canopy turbulence may result in insufficient exchange across the forest-atmosphere boundary exacerbating this condition. Our evaluation of the BASE and MIX turbulence schemes presented in Sect. 3.1 discusses several observed model-measurement discrepancies in BASE-case K_H that are corrected in the MIX scenario, including the two-hour offset between the modeled and measured diurnal cycle of K_H. Overall, this indicates the sensitivity of the top-of-canopy BVOC flux to turbulence and emphasizes the importance of an accurate representation of in-canopy mixing in models.

While enhanced mixing improves the diurnal evolution of isoprene, modeled mixing ratios exceed observations on the second day by 1–3 ppbv, likely due to an underestimate of isoprene oxidation. Oxidation of isoprene in the model is primarily controlled by reaction with OH, with loss rates in the model peaking at midday around 11 pptv min^{-1} (Fig. 5). Oxidation by ozone follows at much smaller rates (up to 2 pptv min^{-1} around sunset) and small contributions by loss with the nitrate radical at night (approximately 0.5 pptv min^{-1}). Simulated NO_3 mixing ratios at 34 m (not shown) peak at 4 pptv the first night under elevated NO_2 concentrations from regional transport and decrease to 0.3 pptv on the second night when chemistry is dominated by local emissions. Past estimates of NO_3 at PROPHET range from 0.4 pptv (Pratt et al., 2012) to 2–3 pptv (Faloona et al., 2001), although we note that NO_3 has not been measured at the site before, making it is difficult to evaluate the model. The primary model NO_3 source is the

ACPD
12, 12801–12852, 2012

nighttime oxidation of NO_2 by O_3, yet observed NO_2 concentrations at the site remain relatively low; therefore, we should expect relatively low concentrations of NO_3 and low isoprene-NO_3 oxidation rates. A potential explanation for the lack of nighttime oxidation may be OH concentrations, as discussed in Sect. 3.4.

Monoterpenes ($C_{10}H_{16}$) are grouped together as a total monoterpene concentration by the PTR-MS. As noted at other forest sites (Bouvier-Brown et al., 2009), observations show a different diurnal cycle than isoprene. The early morning and late evening peak (Fig. 4) and higher concentrations at night than during the day have been attributed to high photooxidation during the daytime and an accumulation at night as these temperature-dependent emissions continue in the absence of sunlight. Above the canopy, higher concentrations of monoterpenes are observed at the beginning of the simulation, suggesting a potential advective source of terpenes to the site in the first six hours of the simulation, which is consistent with air traveling over the forested state. RACM-MIM simulates terpene concentrations to be very similar to the RACM case due to NO changes in the MIM terpene oxidation scheme. As with isoprene, however, enhanced mixing greatly improves the model-measurement agreement in terms of magnitude of concentrations, though the diurnal cycle is only weakly captured.

Formaldehyde (HCHO) is an important VOC oxidation product and is typically produced in relatively large quantities from the oxidation of isoprene. While anthropogenic VOC can also provide a substantial source of HCHO (Pang et al., 2009), their effect on local HCHO concentrations observed at the PROPHET site is minor (Sumner et al., 2001) unless under advective conditions from the south. Observed mixing ratios at the site are 0.5–1 ppbv (Fig. 6), reflecting values that are slightly lower than the 1999 field campaign observations (0.5–12 ppbv, Sumner et al., 2001), consistent with the expected reduced photochemistry in the summer of 2009. An advection source is apparent at the beginning of the simulation with higher HCHO concentrations both above and below the canopy. When an advective HCHO source is added at 45–106 m, measured-modeled comparisons improve above the canopy but not below the canopy, suggesting either that there is in-canopy production that the model does not capture or mixing from

ACPD
12, 12801–12852, 2012

aloft is stronger than simulated. HCHO midday deposition velocity is higher than other studies (2.3 $cm\,s^{-1}$ in our model as compared to 1.5 $cm\,s^{-1}$ in Sumner et al., 2001), yet the model still overestimates HCHO in in all simulations at all heights. HCHO deposition velocity decreases by less than 0.1 $cm\,s^{-1}$ with enhanced mixing, as with that of O_3. When advection is not playing a role (the second day of the simulation), modeled HCHO exhibits a diurnal cycle with higher concentrations during the day especially in the BASE and MIM cases. Both above and below the canopy, the change to MIM increases midday HCHO concentrations by about 15 % due to larger HCHO yields from BVOC oxidation (Geiger et al., 2003). MIM makes additional HCHO from the isoprene peroxy self-reaction (ISOP+ISOP), plus the new methacrolein peroxy radicals (MACP). Enhanced mixing (MIX and MIX+MIM) weakens the diurnal pattern of HCHO, better reflecting observations.

Other key BVOC oxidation products are the lumped species methacrolein and methyl vinyl ketone (MACR + MVK or C_4H_6O). These compounds are detected at the same nominal mass on the PTR-MS and are also lumped in the RACM mechanism. Observed concentrations peak in the early portion of the run both above and below the canopy (Fig. 6) due to advection of oxidation products from the south. Adding an advective source of MACR aloft improves measured-modeled agreement at the beginning of the simulation at all measurement heights. The MIX case improves concentrations as compared to observations, yet removes the observed diurnal pattern. Changing to the MIM mechanism doubles the BASE-case concentrations of MACR + MVK due to the increased yield in MACR + MVK by the reaction of first-generation oxidation products of isoprene with NO. Consequently, modeled concentrations of the MACR RACM-MIM surrogate overestimate measured MACR + MVK by a factor of three throughout the profile. This finding is consistent with chamber study comparisons of RACM and RACM-MIM by Geiger et al. (2003), who attribute the result to measurements only accounting for MACR + MVK while the RACM species also includes all other unsaturated C_4 carbonyls. Past studies suggest that dry deposition rates for MACR + MVK may be underestimated (Pugh et al., 2010), yet the modeled MACR + MVK deposition velocity

ACPD
12, 12801–12852, 2012

of 1.6 cm s^{-1} compares well with observations by Misztal et al. (2011, 1–2 cm s^{-1}). Enhanced mixing reduces the MACR deposition velocity by about 5 %.

We also evaluate the simulation of the biogenic oxidation product hydroxyacetone ($C_3H_6O_2$) added to the RACM-MIM mechanism (denoted as HACE) representing a major product of MACR + MVK oxidation. While calibrated observations of HACE are not available, the model simulates a diurnal cycle with mixing ratios ranging up to 100 pptv that decrease slightly with increased mixing (Fig. 6), which is slightly lower than the range of the uncalibrated measurements (200–500 pptv).

Glyoxal (GLY) was also measured at the site, with mixing ratios reaching up to 25 pptv during midday, and with a clear advective signal on the first day of the simulations (Fig. S3). However, both RACM versions only form GLY from anthropogenic precursors and do not include the production from any biogenic species; therefore, modeled mixing ratios are on the order of 0.01–1 pptv. Observations of GLY suggest local biogenic production of GLY, a source that could be included in future models.

We compare the daytime (11:00–17:00 EST) ratios of (MACR + MVK)/isoprene and HACE/(MACR + MVK) to evaluate the ability of the mechanisms to reproduce observed BVOC oxidation. Over the full field campaign (not shown), the observed (MACR + MVK)/isoprene ratio is 0.18, substantially lower than observed in the Amazon (0.44, Karl et al., 2009), yet comparable to observations from previous PROPHET studies (0.12, Apel et al., 2002). At the PROPHET site, however, the correlation between MACR + MVK and isoprene is weak ($r^2 = 0.03$) as a result of highly variable MACR + MVK advection with respect to wind direction; therefore, the lower ratio observed at the PROPHET site is reasonable given this degree of uncertainty. Figure 7 compares the observed daytime ratios against the four model scenarios for the second day (5 August) to examine local chemistry in the absence of pollution transport. The observed (MACR + MVK)/isoprene ratio of 0.03 is much lower than the mean daytime ratio for the full campaign (0.18) due to decreased advection of MACR + MVK. The BASE and MIM scenarios yield negative ratios, indicating inefficient oxidation of isoprene. This is consistent with the overestimation of isoprene by the BASE and

ACPD
12, 12801–12852, 2012

MIM cases, particularly on the second day, as a result of inefficient mixing out of the canopy. In these scenarios, OH is depleted before isoprene is completely oxidized, leading to insufficient production of MACR + MVK given the amount of isoprene available. With enhanced mixing (MIX and MIX + MIM scenarios), isoprene is oxidized more effectively leading to ratios that correlate well with observations. Additionally, the HACE/(MACR + MVK) relationship can highlight the added oxidation capacity when including the new MACR oxidation pathways in MIM. For local conditions on 5 August, the modeled ratios are 0.08 and 0.09 for the MIM and MIX + MIM cases, respectively, both of which are substantially lower than observed in the Amazon (0.3, Karl et al., 2009) due to lower oxidant concentrations. While the MIX + MIM case ratios are lower than the MIM, we note that the correlation is weaker in the MIX+MIM case (r^2 = 0.57) than the MIM case (r^2 = 0.67), indicating a large uncertainty with these ratios.

To summarize, the original CACHE BASE simulations strongly overestimate isoprene concentrations, particularly in the early evening and at nighttime. This is a known problem in models that occurs at all scales (e.g., 1-D models, 3-D models, etc.) and we attribute this increase at the end of the day to improper mixing in the model. The revised mixing scheme, which is based on observed friction velocities and vertical velocity standard deviations, greatly improves the simulation of primary BVOC at most model levels. Previously, other studies have attributed measured-modeled discrepancies to boundary layer dynamics, but our results suggest an important contribution from forest-canopy exchange. Oxidation products such as HCHO and MACR + MVK are overestimated by the BASE model simulations, with the greatest measured-modeled improvement resulting from the change in mixing parameterization versus the chemical mechanism. In general, the more detailed biogenic oxidation scheme (RACM-MIM) increases the oxidation products to three times more than observed, although the mechanism does improve modeled HO_x as will be discussed in the next section.

ACPD
12, 12801–12852, 2012

3.4 HO_x and OH reactivity

Modeled OH concentrations reproduce the diurnal cycle and magnitude of observed OH (1–2.5 × 10^6 molecules cm^{-3} at midday) (Fig. 8). Difficulties associated with transmission of laser power to the top of the tower led to few measurements of OH greater than the limit of the detection of the instrument (approximately 1 × 10^6 molecules cm^{-3}) during this time period; therefore, Fig. 8 displays an average diurnal cycle of OH of the two simulation days with a peak value of 2 × 10^6 molecules cm^{-3}. The model produces higher OH concentrations on the first day of simulation due to the higher oxidation from incoming advection, while modeled concentrations on the second day are approximately half the observed values. The MIX and MIM cases decrease modeled OH by about 10 and 20 %, respectively, on the first day, and on day two, MIX increases modeled OH by about 10 %. From the vertical profiles (Fig. 9), in-canopy OH concentrations are low, suggesting small OH production rates. OH concentrations are highest above the canopy where substantial production from O_3 photolysis and subsequent reaction with H_2O occurs. In general, enhanced mixing increases the modeled OH concentrations at all heights, whereas the change from RACM to RACM-MIM decreases OH from the surface to 3 h. An exception is during the anthropogenic advection event on the morning of 4 August, when enhanced mixing increases above canopy OH and decreases OH within the canopy; implementing RACM-MIM increases OH throughout the column, due to increased production from the HO_2 + NO reaction.

For HO_2, the measurements show a strong diurnal cycle that is reproduced by the model (Fig. 8). In general, the model underestimates HO_2 in the BASE case simulation, with a slight increase in HO_2 from the MIM simulation. However, recent studies suggest that the detection of HO_2 radicals using chemical conversion to OH by reaction with added NO may be sensitive to the detection of a fraction of hydroxyalkyl peroxy radicals produced from the OH-initiated oxidation of alkenes (Fuchs et al., 2011). Calibrations of the Indiana University FAGE instrument indicate that approximately 90 % of isoprene-based hydroxyalkyl peroxy radicals are detected in addition to HO_2, while only 5 % of

ACPD
12, 12801–12852, 2012

propane-based alkyl peroxy radicals are detected. Given that isoprene dominates the HO_2 radical chemistry at this site, the measured HO_2 concentrations (HO_2^*) likely reflect the sum of both HO_2 and isoprene peroxy radicals (ISOP). In Fig. 8, we compare measured HO_2^* with a similar metric from the model ($HO_2^* = HO_2 + ISOP$) and this greatly improves measured-modeled agreement. The increase in late evening modeled HO_2^* is due to an accumulation of the ISOP radicals, an artifact from the end-of-day increase in isoprene concentrations (see Sect. 3.3). When changing to MIM the explicit treatment of ISOP leads to greater destruction (e.g., the reaction rate for HO_2^* increases, as does the explicit reaction of ISOP+ISOP) and provides better measured-modeled agreement. In the vertical profiles (Fig. 9), the model produces a strong source of HO_2 above the canopy with some in-canopy production. RACM-MIM increases HO_2 throughout the vertical profile, particularly in the daytime. The enhanced mixing (MIX case) increases both in- and above-canopy HO_2 concentrations in the morning and above the canopy during the night. Otherwise, slight decreases in HO_2 occur. During the advection event on 4 August, increased NO_x leads to decreased HO_2 in both the MIX and MIM cases due to loss with NO.

OH reactivity (R_{OH}) represents the total first order loss rate of OH (inverse of the OH lifetime). Measured R_{OH} values during CABINEX 2009 range from 0–2 s^{-1} at night to up to 10 s^{-1} during the day (Fig. 10, left panel), which compare well with previous measurements at PROPHET (Di Carlo et al., 2004). Modeled R_{OH} is calculated by summing the product of the rate constant and reactant concentrations for all species that consume OH. Modeled R_{OH} compares best with observations for the MIX scenario, due to the poor reproduction of the observed diurnal cycle of isoprene simulated by the BASE and MIM simulations. This again suggests the dependence of modeled R_{OH} on the vertical mixing in the model. For modeled R_{OH}, we speciate contributions from BVOC (isoprene, API, LIM) and oxidation productions (HCHO and MACR + MVK). During the afternoon, BVOC account for approximately 85 % of the reactivity in the model, followed by the CO at 15 %, whereas the oxidation products and CO dominate at night and in the early morning (Fig. 10, right panel). Contributions from methane and NO_2 are relatively

ACPD
12, 12801–12852, 2012

small. Kim et al. (2011) note that the oxidation products can account for about 8 % of the reactivity if NO concentrations are low. However, as noted by Kim et al. (2011) and Karl et al. (2009), the R_{OH} tends to increase when photochemically aged air masses arrive at the observation site, which is evident on the first day of the simulation. Because we are including the advection of some primary anthropogenic and secondary oxidation products (Table 1), we correctly model this increase in R_{OH} on the first day of simulation. The second day of the simulation reflects the local conditions, with slightly lower R_{OH} that is slightly overestimated by the model.

4 Summary and conclusions

This manuscript presents results from a 1-D canopy-chemistry model, CACHE, applied to a northern Michigan mixed hardwood forest to elucidate in-canopy atmospheric chemistry during the CABINEX 2009 field campaign. CACHE calculates vertical mixing within and above the forest canopy using K-theory, a parameterization used by many 1-D and 3-D models despite its limitations in the canopy roughness layer. Chemical transformation is modeled using RACM, a condensed mechanism that can cover a broad range of chemical situations but with limited BVOC chemistry. In this study, we test the model sensitivity of vertical gradients of BVOC and their oxidation products to (1) turbulent exchange and (2) chemistry. First, we account for turbulence in the canopy roughness layer by applying the modified K-theory parameterization of Makar et al. (1999) and adjusting the model with high-time-resolution sonic anemometer measurements of friction velocity and vertical velocity standard deviation. Second, we implement an expanded version of RACM with more explicit BVOC chemistry, RACM-MIM.

Traditional K-theory (i.e., BASE) underestimates forest canopy exchange by 0.5–2 orders of magnitude, leading to overly-strong diurnal cycle of ozone, and overestimations in NO_x, BVOC and their oxidation products that accumulate within and above the canopy to 2–3 times higher than observed. In addition, traditional K-theory, in which turbulence is driven by a prognostic temperature profile, does not capture the observed

ACPD
12, 12801–12852, 2012

gradual onset and termination of convective mixing due to a lack of surface heat storage in the model. This leads to anomalous spikes in primary BVOC near the canopy, particularly around sunset, that are not present in the observations. Driving near-canopy vertical mixing with micrometeorological observations (e.g., MIX) improves the representation of vertical mixing as evidenced in the improved vertical profiles and diurnal cycles of BVOC and their oxidation products. While this parameterization cannot account for coherent structures and other non-Fickian diffusion processes, this method provides substantial improvement in the model simulations. Adding additional BVOC oxidation pathways with the RACM-MIM mechanism slightly increases isoprene and HCHO (15 %) with greater changes in MACR + MVK (80 %), although these concentrations were about five times higher than observed at all heights. Past research suggests that MACR + MVK may constitute only a fraction of the MACR RACM surrogate, and that models may underestimate MACR + MVK surface deposition; however, deposition velocity for MACR + MVK in the model compares well with observations. Changes in O_3 and NO_x concentrations with enhanced isoprene chemistry were negligible. Overall, it is evident from this study that BVOC and their oxidation products are more sensitive to turbulence than enhanced isoprene chemistry.

The impact of vertical mixing on HO_x chemistry is dependent on the advection conditions. Advection from polluted regions (e.g., the first day of our simulation) increases OH in the region of advection (45–106 m) and decreases OH below the level of advection. When local chemistry dominates, an increase in mixing increases OH concentrations suggesting that the canopy can be a HO_x source. For HO_2, an increase in mixing tends to decrease concentrations regardless of advection conditions. With changes to the RACM-MIM chemistry, OH decreases due to increased secondary oxidation of biogenic oxidation products and HO_2 decreases throughout the profile. While the additional BVOC oxidation pathways of RACM-MIM improve HO_2, the overestimation of MACR + MVK suggests that the mechanism pathway may not be properly capturing the oxidation of the biogenic oxidation products. Additionally, we find that GLY is

ACPD
12, 12801–12852, 2012

underestimated in the model by an order of magnitude (Fig. S3), suggesting a missing primary biogenic source.

Typically, 1-D models are subject to several aspects of uncertainty, including (1) the emissions from the canopy, (2) the chemistry occurring and the chemical mechanism used, (3) the turbulent mixing, and (4) surface deposition. We have evaluated each of these aspects in this paper, while focussing our sensitivity study on mixing and chemistry. The BVOC emissions have been fairly well-constrained by multiple measurements at the site; however, we find that observed emission factors for isoprene are likely on the lower end of the spectrum due to the unusually cool summer at UMBS. If emission rates were higher than modeled in this study, BVOC concentrations accumulate in the model to unrealistic concentrations. In theory, this could be matched by higher reactivity in the forest, with increased oxidation by OH or NO. We tested the sensitivity of the model to higher NO_x, potentially from a local or advective source by increasing NO_2 advection rates until the NO_x concentrations match urban levels (not shown). With higher isoprene emissions (e.g., the mean value of Ortega et al., 2007), higher NO_x can increase the oxidation and reduce BVOC concentrations to observed values, however modeled NO_x concentrations then exceed observed values by an order of magnitude. It is also possible that OH concentrations are too low in the model (e.g., Fig. 8, left panel); however, our modeled BVOC oxidation products are already higher than observed and we have good measured-modeled agreement in OH reactivity. Therefore, we have evidence to show that the modeled emissions and chemistry balance in the model represents the observed conditions fairly accurately.

Overall, we find that an improved representation of in-canopy turbulent transport based on micrometeorological observations and a consideration for near-field effects improves the simulation of concentrations and vertical gradients of BVOC and their oxidation products observed during the CABINEX 2009 campaign. The change to a mechanism with more specific BVOC pathways slightly improves agreement with observations for HO_2, but produces more BVOC oxidation products than observed (e.g., HCHO, MACR + MVK). While the yields of BVOC oxidation products in MIM may be

ACPD
12, 12801–12852, 2012

too high (e.g., Geiger et al., 2003) or surface deposition rates may be too low (Pugh et al., 2010), observed concentrations of these primary oxidation products suggest that our in-canopy oxidation is within the observational constraints. However, we note that implementation of other isoprene oxidation mechanisms may yield different results. Our results show that mixing in the canopy may be more important than changes to BVOC chemistry mechanisms for accurate modeling of BVOC chemistry and forest-atmosphere exchange, and point to the need for a revised in-canopy turbulence parameterization in existing 1-D and 3-D atmospheric models. A thorough intercomparison of turbulence and BVOC chemistry data from a variety of forest ecosystems is required to assess the applicability of our results on the global scale. Other aspects of the forest canopy, including the turbulence structure of the lower canopy and the effect of vertical heterogeneity of vegetation (i.e., an understory and overstory of differing plant type) on the oxidation capacity of the canopy and forest-atmosphere exchange of BVOC may provide further information for understanding the vertical profiles of BVOC, their oxidation products, and their contribution to tropospheric chemistry.

Supplementary material related to this article is available online at: http://www.atmos-chem-phys-discuss.net/12/12801/2012/acpd-12-12801-2012-supplement.pdf.

Acknowledgements. Funding for this work was provided by the National Science Foundation AGS-0904128 to M. A. Carroll and A. L. Steiner at the University of Michigan (UM). Additional support for A. M. Bryan was provided through the University of Michigan Elizabeth C. Crosby Research Foundation and the Michigan Space Grant Consortium. We thank C. Vogel at UMBS for providing ancillary meteorological data for our analysis, as well as Meghan Thurlow, Melissa Galloway, and Anthony O'Brien for providing the glyoxal measurements.

ACPD
12, 12801–12852, 2012

References

Alaghmand, M., Shepson, P. B., Starn, T. K., Jobson, B. T., Wallace, H. W., Carroll, M. A., Bertman, S. B., Lamb, B., Edburg, S. L., Zhou, X., Apel, E., Riemer, D., Stevens, P., and Keutsch, F.: The Morning NO_x maximum in the forest atmosphere boundary layer, Atmos. Chem. Phys. Discuss., 11, 29251–29282, doi:10.5194/acpd-11-29251-2011, 2011. 12816, 12820

Apel, E. C., Riemer, D. D., Hills, A., Baugh, W., Orlando, J., Faloona, I., Tan, D., Brune, W., Lamb, B., Westberg, H., Carroll, M. A., Thornberry, T., and Geron, C. D.: Measurement and interpretation of isoprene fluxes and isoprene, methacrolein, and methyl vinyl ketone mixing ratios at the PROPHET site during the 1998 Intensive, J. Geophys. Res., 107, 4034, doi:10.1029/2000JD000225, 2002. 12824

Asner, G. P.: Biophysical and Biochemical Sources of Variability in Canopy Reflectance, Remote Sens. Environ., 64, 234–253, doi:10.1016/S0034-4257(98)00014-5, 1998. 12814, 12842

Baldocchi, D.: A multi-layer model for estimating sulfur dioxide deposition to a deciduous oak forest canopy, Atmos. Environ., 22, 869–884, doi:10.1016/0004-6981(88)90264-8, 1988. 12815

Baldocchi, D., Falge, E., Gu, L., Olson, R., Hollinger, D., Running, S., Anthoni, P., Bernhofer, C., Davis, K., Evans, R., Fuentes, J., Goldstein, A., Katul, G., Law, B., Lee, X., Malhi, Y., Meyers, T., Munger, W., Oechel, W., Paw U, K. T., Pilegaard, K., Schmid, H. P., Valentini, R., Verma, S., Vesala, T., Wilson, K., and Wofsyn, S.: FLUXNET: A New Tool to Study the Temporal and Spatial Variability of Ecosystem-Scale Carbon Dioxide, Water Vapor, and Energy Flux Densities, B. Am. Meteor. Soc., 82, 2415–2434, 2001. 12808

Barkley, M. P., Palmer, P. I., Ganzeveld, L., Arneth, A., Hagberg, D., Karl, T., Guenther, A., Paulot, F., Wennberg, P. O., Mao, J., Kurosu, T. P., Chance, K., Müller, J.-F., De Smedt, I., Van Roozendael, M., Chen, D., Wang, Y., and Yantosca, R. M.: Can a "state of the art" chemistry transport model simulate Amazonian tropospheric chemistry?, J. Geophys. Res., 116, D16302, doi:10.1029/2011JD015893, 2011. 12804, 12820

Blackadar, A. K.: High-resolution models of the planetary boundary layer, in: Advances in Environmental Science and Engineering, Gordon and Breech Science Publishers, Inc., New York, 1, 50–85, 1979. 12805

Bouvier-Brown, N. C., Goldstein, A. H., Gilman, J. B., Kuster, W. C., and de Gouw, J. A.: In-situ ambient quantification of monoterpenes, sesquiterpenes, and related oxygenated

ACPD
12, 12801–12852, 2012

compounds during BEARPEX 2007: implications for gas- and particle-phase chemistry, Atmos. Chem. Phys., 9, 5505–5518, doi:10.5194/acp-9-5505-2009, 2009. 12822

Boy, M., Sogachev, A., Lauros, J., Zhou, L., Guenther, A., and Smolander, S.: SOSA – a new model to simulate the concentrations of organic vapours and sulphuric acid inside the ABL – Part 1: Model description and initial evaluation, Atmos. Chem. Phys., 11, 43–51, doi:10.5194/acp-11-43-2011, 2011. 12806

Butler, T. M., Taraborrelli, D., Brühl, C., Fischer, H., Harder, H., Martinez, M., Williams, J., Lawrence, M. G., and Lelieveld, J.: Improved simulation of isoprene oxidation chemistry with the ECHAM5/MESSy chemistry-climate model: lessons from the GABRIEL airborne field campaign, Atmos. Chem. Phys., 8, 4529–4546, doi:10.5194/acp-8-4529-2008, 2008. 12804, 12811

Carlton, A. G., Wiedinmyer, C., and Kroll, J. H.: A review of Secondary Organic Aerosol (SOA) formation from isoprene, Atmos. Chem. Phys., 9, 4987–5005, doi:10.5194/acp-9-4987-2009, 2009. 12804

Carroll, M. A., Bertman, S. B., and Shepson, P. B.: Overview of the Program for Research on Oxidants: PHotochemistry, Emissions, and Transport (PROPHET) summer 1998 measurements intensive, J. Geophys. Res., 106, 24275–24288, 2001. 12804, 12806

Carslaw, N. and Carslaw, D.: The gas-phase chemistry of urban atmospheres, Surv. Geophys., 22, 31–53, 2001. 12804

Claeys, M., Graham, B., Vas, G., Wang, W., Vermeylen, R., Pashynska, V., Cafmeyer, J., Guyon, P., Andreae, M. O., Artaxo, P., and Maenhaut, W.: Formation of Secondary Organic Aerosols Through Photooxidation of Isoprene, Science, 303, 1173–1176, doi:10.1126/science.1092805, 2004. 12804

Collineau, S. and Brunet, Y.: Detection of turbulent coherent motions in a forest canopy part II: Time-scales and conditional averages, Bound.-Lay. Meteor., 66, 49–73, doi:10.1007/BF00705459, 1993. 12811

Cooper, O. R., Moody, J. L., Thornberry, T. D., Town, M. S., and Carroll, M. A.: PROPHET 1998 meteorological overview and air-mass classification, J. Geophys. Res., 106, 24289–24299, 2001. 12813

de Gouw, J. and Warneke, C.: Measurements of volatile organic compounds in the Earth's atmosphere using proton-transfer-reaction mass spectrometry, Mass. Spectrom. Rev., 26, 223–257, 2007. 12808

ACPD
12, 12801–12852, 2012

Di Carlo, P., Brune, W. H., Martinez, M., Harder, H., Lesher, R., Ren, X., Thornberry, T., Carroll, M. A., Young, V., Shepson, P. B., Riemer, D., Apel, E., and Campbell, C.: Missing OH Reactivity in a Forest: Evidence for Unknown Reactive Biogenic VOCs, Science, 304, 722–725, doi:10.1126/science.1094392, 2004. 12806, 12827

Dusanter, S., Vimal, D., Stevens, P. S., Volkamer, R., and Molina, L. T.: Measurements of OH and HO_2 concentrations during the MCMA-2006 field campaign – Part 1: Deployment of the Indiana University laser-induced fluorescence instrument, Atmos. Chem. Phys., 9, 1665–1685, doi:10.5194/acp-9-1665-2009, 2009. 12808

Faloona, I., Tan, D., Brune, W., Hurst, J., Barket, Dennis, J., Couch, T. L., Shepson, P., Apel, E., Riemer, D., Thornberry, T., Carroll, M. A., Sillman, S., Keeler, G. J., Sagady, J., Hooper, D., and Paterson, K.: Nighttime observations of anomalously high levels of hydroxyl radicals above a deciduous forest canopy, J. Geophys. Res., 106, 24315–24333, 2001. 12806, 12821

Finkelstein, P. L., Ellestad, T. G., Clarke, J. F., Meyers, T. P., Schwede, D. B., Hebert, E. O., and Neal, J. A.: Ozone and sulfur dioxide dry deposition to forests: Observations and model evaluation, J. Geophys. Res., 105, 15365–15377, 2000. 12819

Finnigan, J.: Turbulence in Plant Canopies, Annu. Rev. Fluid Mech., 32, 519–571, doi:10.1146/annurev.fluid.32.1.519, 2000. 12805, 12811

Forkel, R., Seidl, W., Dlugi, R., and Deigele, E.: A One-Dimensional Numerical-Model to Simulate Formation and Balance of Sulfate during Radiation Fog Events, J. Geophys. Res., 95, 18501–18515, 1990. 12810, 12811, 12816

Forkel, R., Klemm, O., Graus, M., Rappenglück, B., Stockwell, W. R., Grabmer, W., Held, A., Hansel, A., and Steinbrecher, R.: Trace gas exchange and gas phase chemistry in a Norway spruce forest: A study with a coupled 1-dimensional canopy atmospheric chemistry emission model, Atmos. Environ., 40, Supplement 1, 28–42, doi:10.1016/j.atmosenv.2005.11.070, 2006. 12805, 12807, 12809, 12815, 12816, 12820

Fuchs, H., Bohn, B., Hofzumahaus, A., Holland, F., Lu, K. D., Nehr, S., Rohrer, F., and Wahner, A.: Detection of HO_2 by laser-induced fluorescence: calibration and interferences from RO_2 radicals, Atmos. Meas. Tech., 4, 1209–1225, doi:10.5194/amt-4-1209-2011, 2011. 12826

Ganzeveld, L., Klemm, O., Rappenglück, B., and Valverde-Canossa, J.: Evaluation of meteorological parameters over a coniferous forest in a single-column chemistry-climate model, Atmos. Environ., 40, Supplement 1, 21–27, doi:10.1016/j.atmosenv.2006.01.061, 2006. 12806

ACPD
12, 12801–12852, 2012

Gao, W., Wesely, M. L., and Doskey, P. V.: Numerical Modeling of the Turbulent Diffusion and Chemistry of NO_x, O_3, Isoprene, and Other Reactive Trace Gases in and Above a Forest Canopy, J. Geophys. Res., 98, 18339–18353, 1993. 12805

Geiger, H., Barnes, I., Bejan, I., Benter, T., and Spittler, M.: The tropospheric degradation of isoprene: an updated module for the regional atmospheric chemistry mechanism, Atmos. Environ., 37, 1503–1519, doi:10.1016/S1352-2310(02)01047-6, 2003. 12812, 12823, 12831

Goldstein, A. H. and Galbally, I. E.: Known and Unexplored Organic Constituents in the Earth's Atmosphere, Environ. Sci. Technol., 41, 1514–1521, doi:10.1021/es072476p, 2007. 12804

Guenther, A., Hewitt, C. N., Erickson, D., Fall, R., Geron, C., Graedel, T., Harley, P., Klinger, L., Lerdau, M., Mckay, W. A., Pierce, T., Scholes, B., Steinbrecher, R., Tallamraju, R., Taylor, J., and Zimmerman, P.: A global model of natural volatile organic compound emissions, J. Geophys. Res., 100, 8873–8892, 1995. 12804, 12815

Hallquist, M., Wenger, J. C., Baltensperger, U., Rudich, Y., Simpson, D., Claeys, M., Dommen, J., Donahue, N. M., George, C., Goldstein, A. H., Hamilton, J. F., Herrmann, H., Hoffmann, T., Iinuma, Y., Jang, M., Jenkin, M. E., Jimenez, J. L., Kiendler-Scharr, A., Maenhaut, W., McFiggans, G., Mentel, Th. F., Monod, A., Prévôt, A. S. H., Seinfeld, J. H., Surratt, J. D., Szmigielski, R., and Wildt, J.: The formation, properties and impact of secondary organic aerosol: current and emerging issues, Atmos. Chem. Phys., 9, 5155–5236, doi:10.5194/acp-9-5155-2009, 2009. 12804

Hanson, D. T. and Sharkey, T. D.: Rate of acclimation of the capacity for isoprene emission in response to light and temperature, Plant Cell. Environ., 24, 937–946, doi:10.1046/j.1365-3040.2001.00745.x, 2001. 12816

Heus, T., van Heerwaarden, C. C., Jonker, H. J. J., Pier Siebesma, A., Axelsen, S., van den Dries, K., Geoffroy, O., Moene, A. F., Pino, D., de Roode, S. R., and Vilà-Guerau de Arellano, J.: Formulation of the Dutch Atmospheric Large-Eddy Simulation (DALES) and overview of its applications, Geosci. Model Dev., 3, 415–444, doi:10.5194/gmd-3-415-2010, 2010. 12806

Hewitt, C. N., Lee, J. D., MacKenzie, A. R., Barkley, M. P., Carslaw, N., Carver, G. D., Chappell, N. A., Coe, H., Collier, C., Commane, R., Davies, F., Davison, B., DiCarlo, P., Di Marco, C. F., Dorsey, J. R., Edwards, P. M., Evans, M. J., Fowler, D., Furneaux, K. L., Gallagher, M., Guenther, A., Heard, D. E., Helfter, C., Hopkins, J., Ingham, T., Irwin, M., Jones, C., Karunaharan, A., Langford, B., Lewis, A. C., Lim, S. F., MacDonald, S. M., Mahajan, A. S., Malpass, S., McFiggans, G., Mills, G., Misztal, P., Moller, S., Monks, P. S., Nemitz, E., Nicolas-Perea, V., Oetjen, H., Oram, D. E., Palmer, P. I., Phillips, G. J., Pike, R., Plane, J. M.

ACPD
12, 12801–12852, 2012

C., Pugh, T., Pyle, J. A., Reeves, C. E., Robinson, N. H., Stewart, D., Stone, D., Whalley, L. K., and Yin, X.: Overview: oxidant and particle photochemical processes above a south-east Asian tropical rainforest (the OP3 project): introduction, rationale, location characteristics and tools, Atmos. Chem. Phys., 10, 169–199, doi:10.5194/acp-10-169-2010, 2010. 12804

Hofzumahaus, A., Rohrer, F., Lu, K., Bohn, B., Brauers, T., Chang, C.-C., Fuchs, H., Holland, F., Kita, K., Kondo, Y., Li, X., Lou, S., Shao, M., Zeng, L., Wahner, A., and Zhang, Y.: Amplified Trace Gas Removal in the Troposphere, Science, 324, 1702–1704, doi:10.1126/science.1164566, 2009. 12804

Huisman, A. J., Hottle, J. R., Galloway, M. M., DiGangi, J. P., Coens, K. L., Choi, W., Faloona, I. C., Gilman, J. B., Kuster, W. C., de Gouw, J., Bouvier-Brown, N. C., Goldstein, A. H., LaFranchi, B. W., Cohen, R. C., Wolfe, G. M., Thornton, J. A., Docherty, K. S., Farmer, D. K., Cubison, M. J., Jimenez, J. L., Mao, J., Brune, W. H., and Keutsch, F. N.: Photochemical modeling of glyoxal at a rural site: observations and analysis from BEARPEX 2007, Atmos. Chem. Phys., 11, 8883–8897, doi:10.5194/acp-11-8883-2011, 2011. 12808

Hurst, J. M., Barket, Dennis J., J., Herrera-Gomez, O., Couch, T. L., Shepson, P. B., Faloona, I., Tan, D., Brune, W., Westberg, H., Lamb, B., Biesenthal, T., Young, V., Goldstein, A., Munger, J. W., Thornberry, T., and Carroll, M. A.: Investigation of the nighttime decay of isoprene, J. Geophys. Res., 106, 24335–24346, 2001. 12805

Jobson, B. T. and McCoskey, J. K.: Sample drying to improve HCHO measurements by PTR-MS instruments: laboratory and field measurements, Atmos. Chem. Phys., 10, 1821–1835, doi:10.5194/acp-10-1821-2010, 2010. 12808

Karl, T., Guenther, A., Turnipseed, A., Tyndall, G., Artaxo, P., and Martin, S.: Rapid formation of isoprene photo-oxidation products observed in Amazonia, Atmos. Chem. Phys., 9, 7753–7767, doi:10.5194/acp-9-7753-2009, 2009. 12804, 12805, 12824, 12825, 12828

Kim, S., Guenther, A., Karl, T., and Greenberg, J.: Contributions of primary and secondary biogenic VOC tototal OH reactivity during the CABINEX (Community Atmosphere-Biosphere INteractions Experiments)-09 field campaign, Atmos. Chem. Phys., 11, 8613–8623, doi:10.5194/acp-11-8613-2011, 2011. 12807, 12828

Kovacs, T. A. and Brune, W. H.: Total OH Loss Rate Measurement, J. Atmos. Chem., 39, 105–122, doi:10.1023/A:1010614113786, 2001. 12808

Krol, M. C., Molemaker, M. J., and Vilà-Guerau de Arellano, J.: Effects of turbulence and heterogeneous emissions on photochemically active species in the convective boundary layer, J. Geophys. Res., 105, 6871–6884, 2000. 12804

ACPD
12, 12801–12852, 2012

LADCO: Regional Network Assessment: States of Illinois, Indiana, Michigan, Minnesota, Ohio, and Wisconsin, Tech. rep., Lake Michigan Air Directors Consortium (LADCO), Des Plaines, IL, available at: http://www.ladco.org/reports/general/Regional_Network_Assessment/Regional_Network_Assessment_Report_Version_5.0_May_27_2010.pdf, draft report, 27 May, 2010. 12813

Lelieveld, J., Butler, T. M., Crowley, J. N., Dillon, T. J., Fischer, H., Ganzeveld, L., Harder, H., Lawrence, M. G., Martinez, M., Taraborrelli, D., and Williams, J.: Atmospheric oxidation capacity sustained by a tropical forest, Nature, 452, 737–740, 2008. 12804

Logan, J. A.: Tropospheric Ozone: Seasonal Behavior, Trends, and Anthropogenic Influence, J. Geophys. Res., 90, 10463–10482, 1985. 12804

Makar, P. A., Fuentes, J. D., Wang, D., Staebler, R. M., and Wiebe, H. A.: Chemical processing of biogenic hydrocarbons within and above a temperate deciduous forest, J. Geophys. Res., 104, 3581–3603, 1999. 12805, 12810, 12816, 12828

Martin, R. S., Westberg, H., Allwine, E., Ashman, L., Farmer, J. C., and Lamb, B.: Measurement of isoprene and its atmospheric oxidation products in a central Pennsylvania deciduous forest, J. Atmos. Chem., 13, 1–32, doi:10.1007/BF00048098, 1991. 12820

Martin, S. T., Andreae, M. O., Althausen, D., Artaxo, P., Baars, H., Borrmann, S., Chen, Q., Farmer, D. K., Guenther, A., Gunthe, S. S., Jimenez, J. L., Karl, T., Longo, K., Manzi, A., Müller, T., Pauliquevis, T., Petters, M. D., Prenni, A. J., Pöschl, U., Rizzo, L. V., Schneider, J., Smith, J. N., Swietlicki, E., Tota, J., Wang, J., Wiedensohler, A., and Zorn, S. R.: An overview of the Amazonian Aerosol Characterization Experiment 2008 (AMAZE-08), Atmos. Chem. Phys., 10, 11415–11438, doi:10.5194/acp-10-11415-2010, 2010. 12804

Misztal, P. K., Nemitz, E., Langford, B., Di Marco, C. F., Phillips, G. J., Hewitt, C. N., MacKenzie, A. R., Owen, S. M., Fowler, D., Heal, M. R., and Cape, J. N.: Direct ecosystem fluxes of volatile organic compounds from oil palms in South-East Asia, Atmos. Chem. Phys., 11, 8995–9017, doi:10.5194/acp-11-8995-2011, 2011. 12824

Molemaker, M. J. and Vilà-Guerau de Arellano, J.: Control of Chemical Reactions by Convective Turbulence in the Boundary Layer, J. Atmos. Sci., 55, 568–579, 1998. 12804

Ortega, J. and Helmig, D.: Approaches for quantifying reactive and low-volatility biogenic organic compound emissions by vegetation enclosure techniques – Part A, Chemosphere, 72, 343–364, doi:10.1016/j.chemosphere.2007.11.020, 2008. 12815

Ortega, J., Helmig, D., Guenther, A., Harley, P., Pressley, S., and Vogel, C.: Flux estimates and OH reaction potential of reactive biogenic volatile organic compounds

ACPD
12, 12801–12852, 2012

(BVOCs) from a mixed northern hardwood forest, Atmos. Environ., 41, 5479–5495, doi:10.1016/j.atmosenv.2006.12.033, 2007. 12807, 12814, 12815, 12830
Pang, X., Mu, Y., Zhang, Y., Lee, X., and Yuan, J.: Contribution of isoprene to formaldehyde and ozone formation based on its oxidation products measurement in Beijing, China, Atmos. Environ., 43, 2142–2147, doi:10.1016/j.atmosenv.2009.01.022, 2009. 12822
Patton, E., Davis, K., Barth, M., and Sullivan, P.: Decaying Scalars Emitted By A Forest Canopy: A Numerical Study, Bound.-Lay. Meteorol., 100, 91–129, doi:10.1023/A:1019223515444, 2001. 12806
Paulot, F., Crounse, J. D., Kjaergaard, H. G., Kroll, J. H., Seinfeld, J. H., and Wennberg, P. O.: Isoprene photooxidation: new insights into the production of acids and organic nitrates, Atmos. Chem. Phys., 9, 1479–1501, doi:10.5194/acp-9-1479-2009, 2009. 12804, 12805
Peeters, J., Nguyen, T. L., and Vereecken, L.: HO_x radical regeneration in the oxidation of isoprene, Phys. Chem. Chem. Phys., 11, 5935–5939, doi:10.1039/B908511D, 2009. 12805
Perterer, J. and Körner, C.: The problem of reference parameters in physiological-ecological research with conifer needles, Forstwiss. Centralbl., 109, 220–241, 1990. 12815
Pétron, G., Harley, P., Greenberg, J., and Guenther, A.: Seasonal temperature variations influence isoprene emission, Geophys. Res. Lett., 28, 1707–1710, 2001. 12816
Poisson, N., Kanakidou, M., and Crutzen, P. J.: Impact of Non-Methane Hydrocarbons on Tropospheric Chemistry and the Oxidizing Power of the Global Troposphere: 3-Dimensional Modelling Results, J. Atmos. Chem., 36, 157–230, doi:10.1023/A:1006300616544, 2000. 12804
Pöschl, U., von Kuhlmann, R., Poisson, N., and Crutzen, P. J.: Development and Intercomparison of Condensed Isoprene Oxidation Mechanisms for Global Atmospheric Modeling, J. Atmos. Chem., 37, 29–52, doi:10.1023/A:1006391009798, 2000. 12805
Pratt, K. A., Mielke, L. H., Shepson, P. B., Bryan, A. M., Steiner, A. L., Ortega, J., Daly, R., Helmig, D., Vogel, C. S., Griffith, S., Dusanter, S., Stevens, P. S., and Alaghmand, M.: A one-dimensional model study of individual reactive biogenic volatile organic compounds and their contributions to organic nitrates above a mixed forest, Atmos. Chem. Phys. Discuss., in preparation, 2012. 12821
Pressley, S., Lamb, B., Westberg, H., Flaherty, J., Chen, J., and Vogel, C.: Long-term isoprene flux measurements above a northern hardwood forest, J. Geophys. Res., 110, D07301, doi:10.1029/2004JD005523, 2005. 12807

ACPD
12, 12801–12852, 2012

Pugh, T. A. M., MacKenzie, A. R., Hewitt, C. N., Langford, B., Edwards, P. M., Furneaux, K. L., Heard, D. E., Hopkins, J. R., Jones, C. E., Karunaharan, A., Lee, J., Mills, G., Misztal, P., Moller, S., Monks, P. S., and Whalley, L. K.: Simulating atmospheric composition over a South-East Asian tropical rainforest: performance of a chemistry box model, Atmos. Chem. Phys., 10, 279–298, doi:10.5194/acp-10-279-2010, 2010. 12804, 12811, 12823, 12831

Raupach, M. R.: A practical Lagrangian method for relating scalar concentrations to source distributions in vegetation canopies, Q. J. Roy. Meteor. Soc., 115, 609–632, doi:10.1002/qj.49711548710, 1989. 12805

Raupach, M. R., Finnigan, J. J., and Brunei, Y.: Coherent eddies and turbulence in vegetation canopies: The mixing-layer analogy, Bound.-Lay. Meteor., 78, 351–382, doi:10.1007/BF00120941, 1996. 12805

Schmid, H. P., Su, H. B., Vogel, C. S., and Curtis, P. S.: Ecosystem-atmosphere exchange of carbon dioxide over a mixed hardwood forest in northern lower Michigan, J. Geophys. Res., 108, 4417, doi:10.1029/2002JD003011, 2003. 12807

Sillman, S., Carroll, M. A., Thornberry, T., Lamb, B. K., Westberg, H., Brune, W. H., Faloona, I., Tan, D., Shepson, P. B., Sumner, A. L., Hastie, D. R., Mihele, C. M., Apel, E. C., Riemer, D. D., and Zika, R. G.: Loss of isoprene and sources of nighttime OH radicals at a rural site in the United States: Results from photochemical models, J. Geophys. Res., 107, 4043, doi:10.1029/2001JD000449, 2002. 12806, 12813, 12820

Simpson, D., Guenther, A., Hewitt, C. N., and Steinbrecher, R.: Biogenic emissions in Europe 1. Estimates and uncertainties, J. Geophys. Res., 100, 22875–22890, 1995. 12816

Stavrakou, T., Peeters, J., and Müller, J.-F.: Improved global modelling of HO_x recycling in isoprene oxidation: evaluation against the GABRIEL and INTEX-A aircraft campaign measurements, Atmos. Chem. Phys., 10, 9863–9878, doi:10.5194/acp-10-9863-2010, 2010. 12805

Steinbrecher, R., Hauff, K., Hakola, H., and Rössler, J.: A Revised Parametrisation for Emission Modelling of Isoprenoids for Boreal Plants, in: Biogenic VOC emissions and photochemistry in the boreal regions of Europe – Biphorep, edited by: Laurila, T. and Lindfors, V., no. 70 in Air pollution research report, Commission of the European Communities, EUR 18910 EN. EC, Brussels, 29–43, 1999. 12815

Steiner, A. L., Pressley, S. N., Botros, A., Jones, E., Chung, S. H., and Edburg, S. L.: Analysis of coherent structures and atmosphere-canopy coupling strength during the CABINEX field campaign, Atmos. Chem. Phys., 11, 11921–11936, doi:10.5194/acp-11-11921-2011, 2011. 12808

ACPD
12, 12801–12852, 2012

Stevens, P., Mather, J., and Brune, W.: Measurement of tropospheric OH and HO_2 by laser-induced fluorescence at low pressure, J. Geophys. Res., 99, 3543–3557, 1994. 12808

Stockwell, W. R., Kirchner, F., Kuhn, M., and Seefeld, S.: A new mechanism for regional atmospheric chemistry modeling, J. Geophys. Res., 102, 25847–25879, 1997. 12812, 12813

Stroud, C., Makar, P., Karl, T., Guenther, A., Geron, C., Turnipseed, A., Nemitz, E., Baker, B., Potosnak, M., and Fuentes, J. D.: Role of canopy-scale photochemistry in modifying biogenic-atmosphere exchange of reactive terpene species: Results from the CELTIC field study, J. Geophys. Res., 110, D17303, doi:10.1029/2005JD005775 2005. 12805, 12811, 12819

Stull, R. B.: An Introduction to Boundary Layer Meteorology, Kluwer Academic Publishers, Dordrecht/Boston/London, 1988. 12815

Sumner, A. L., Shepson, P. B., Couch, T. L., Thornberry, T., Carroll, M. A., Sillman, S., Pippin, M., Bertman, S., Tan, D., Faloona, I., Brune, W., Young, V., Cooper, O., Moody, J., and Stockwell, W.: A study of formaldehyde chemistry above a forest canopy, J. Geophys. Res., 106, 24387–24405, 2001. 12822, 12823

Tan, D., Faloona, I., Simpas, J. B., Brune, W., Shepson, P. B., Couch, T. L., Sumner, A. L., Carroll, M. A., Thornberry, T., Apel, E., Riemer, D., and Stockwell, W.: HO_x budgets in a deciduous forest: Results from the PROPHET summer 1998 campaign, J. Geophys. Res., 106, 24407–24427, 2001. 12804, 12806

Wolfe, G. M. and Thornton, J. A.: The Chemistry of Atmosphere-Forest Exchange (CAFE) Model – Part 1: Model description and characterization, Atmos. Chem. Phys., 11, 77–101, doi:10.5194/acp-11-77-2011, 2011. 12805, 12811

Wolfe, G. M., Thornton, J. A., Bouvier-Brown, N. C., Goldstein, A. H., Park, J.-H., McKay, M., Matross, D. M., Mao, J., Brune, W. H., LaFranchi, B. W., Browne, E. C., Min, K.-E., Wooldridge, P. J., Cohen, R. C., Crounse, J. D., Faloona, I. C., Gilman, J. B., Kuster, W. C., de Gouw, J. A., Huisman, A., and Keutsch, F. N.: The Chemistry of Atmosphere-Forest Exchange (CAFE) Model – Part 2: Application to BEARPEX-2007 observations, Atmos. Chem. Phys., 11, 1269–1294, doi:10.5194/acp-11-1269-2011, 2011. 12806, 12819

ACPD

12, 12801–12852, 2012

Table 1. Advection rates for NO_x, VOC, and other hydrocarbons as a function of wind direction. Rates (in ppbv h^{-1}) are scaled by the geostrophic wind speed.

RACM species name	90–135°, 225–270°	135–225°
NO_2	0.05	0.25
MACR	0.00	1.00
HCHO (anthropogenic)	0.00	0.03
HCHO (biogenic)	0.00	1.00
KET	0.00	0.25
HC3	0.00	2.50×10^{-4}
HC5	0.00	0.25
OLT	0.00	0.13
OLI	0.00	0.01

ACPD
12, 12801–12852, 2012

Table 2. Leaf and soil reflectance and transmittance by waveband (visible/near infrared/thermal) used in CACHE. Absorptivities are 1 – (reflectance + transmittance). Values are derived from Asner (1998).

	Soil	Leaf
Reflectance	0.15/0.20/0.10	0.20/0.45/0.10
Transmittance	0.00/0.00/0.00	0.10/0.30/0.10

ACPD
12, 12801–12852, 2012

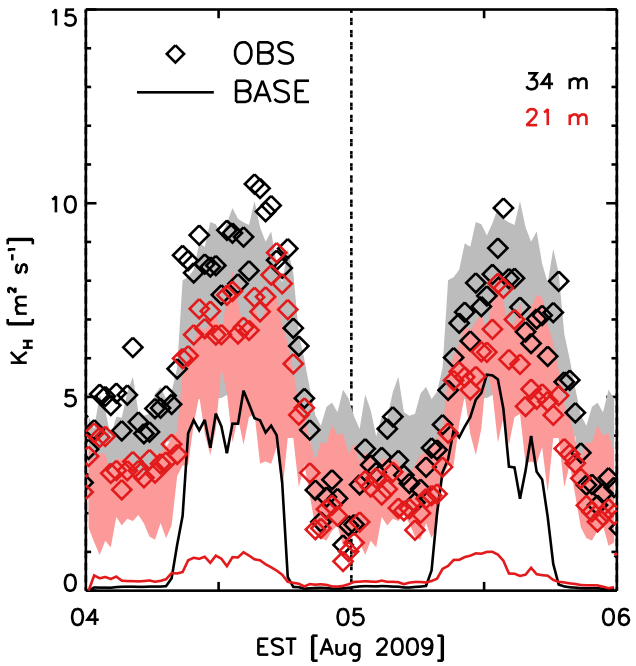

Fig. 1. Measured and modeled (BASE) time series of the turbulent exchange coefficient (K_H) in the upper-canopy (20.6 m, 0.92 h) and above the canopy (34 m, 1.92 h) for 4–5 August 2009. Standard deviations of the mean diurnal cycle for the sunny and partly sunny days (21, 29 July, 2, 4, 5, and 7 August) are shaded. Observed K_H are calculated using sonic anemometer estimations of u^* and σ_w.

ACPD
12, 12801–12852, 2012

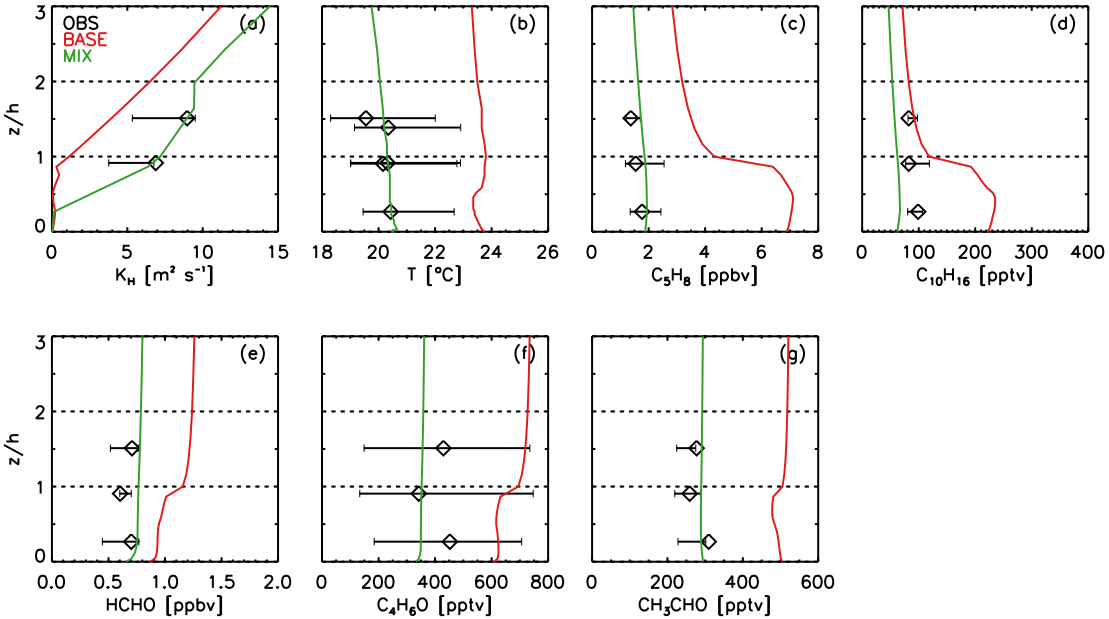

Fig. 2. Measured and modeled vertical profiles of **(a)** eddy diffusivity, **(b)** temperature, **(c)** isoprene, **(d)** monoterpenes, **(e)** formaldehyde, **(f)** MACR + MVK, and **(g)** acetaldehyde at 14:00 EST 5 August 2009. Whiskers denote the standard deviations for the sunny and partly sunny days (21, 29 July, 2, 4, 5, and 7 August).

ACPD
12, 12801–12852, 2012

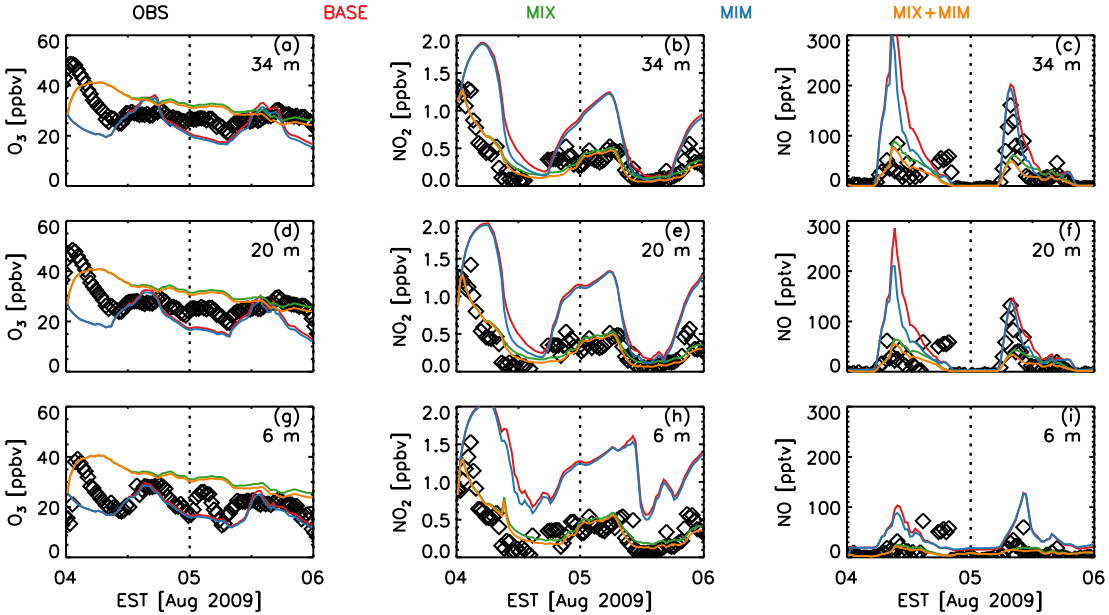

Fig. 3. Measured versus modeled time series for **(a, d, g)** O_3, **(b, e, h)** NO_2, and **(c, f, i)** NO at 34 m, 20.4 m, and 6 m for the 4–5 August 2009 simulation period.

ACPD
12, 12801–12852, 2012

Modeling in-canopy chemistry during CABINEX 2009

A. M. Bryan et al.

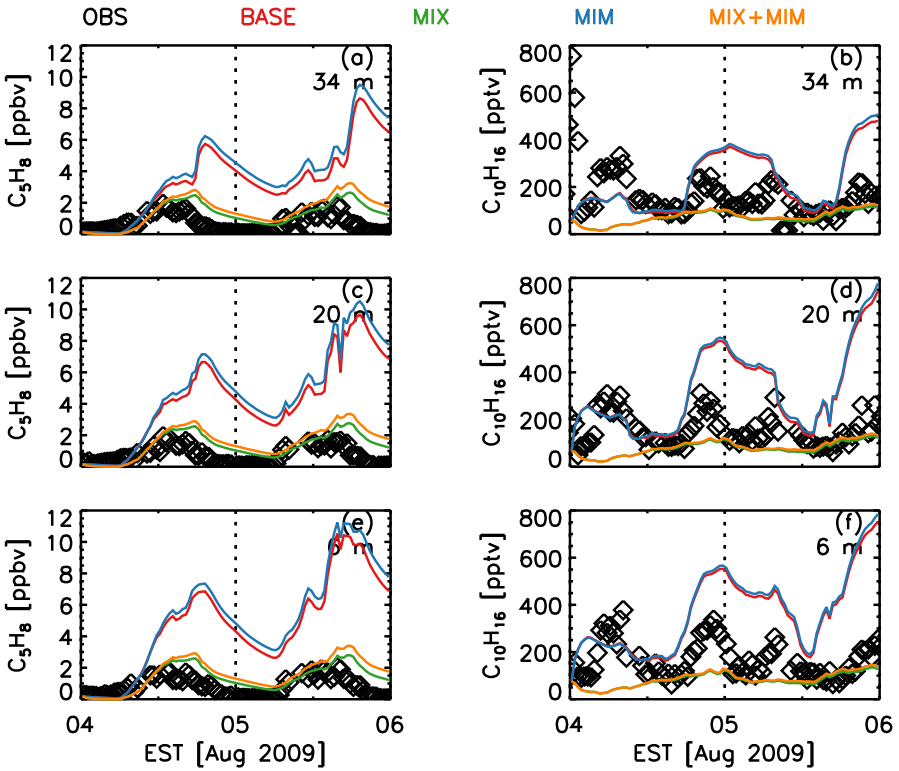

Fig. 4. Same as Fig. 3, but for **(a, c, e)** isoprene and **(b, d, f)** monoterpenes.

ACPD
12, 12801–12852, 2012

Modeling in-canopy chemistry during CABINEX 2009

A. M. Bryan et al.

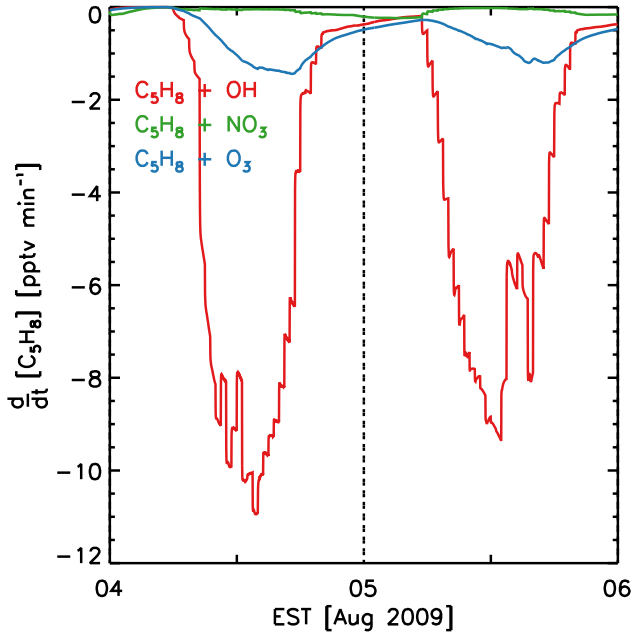

Fig. 5. Modeled isoprene loss rates with respect to reaction with OH, NO_3, and O_3 at 34 m from the MIX case.

ACPD
12, 12801–12852, 2012

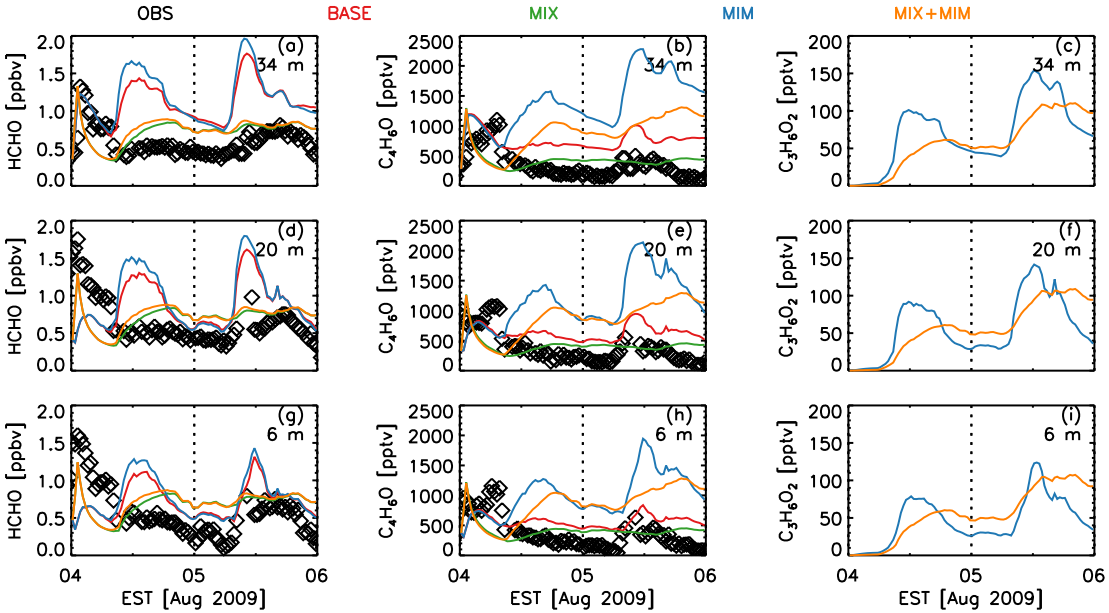

Fig. 6. Same as Fig. 3, but for **(a, d, g)** formaldehyde, **(b, e, h)** MACR + MVK, and **(c, f, i)** hydroxyacetone. Observations of hydroxyacetone are not available.

ACPD
12, 12801–12852, 2012

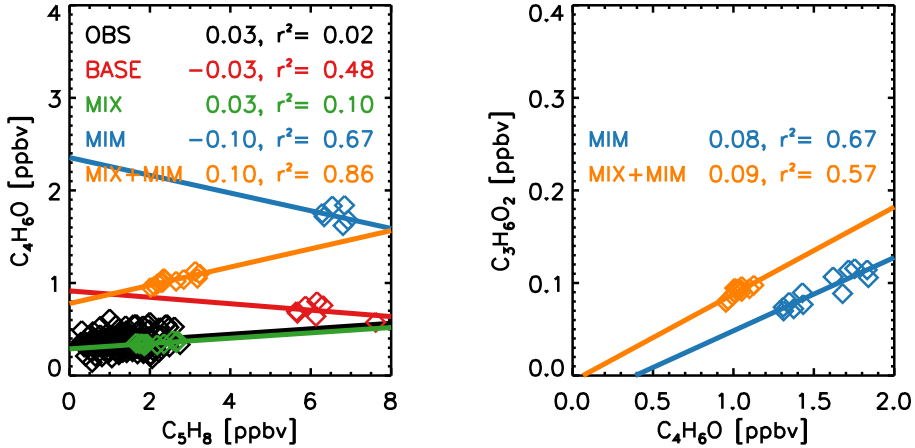

Fig. 7. Measured and modeled correlations between MACR + MVK and isoprene (left), and hydroxyacetone and MACR + MVK (right) at 34 m for 5 August 2009 between 11:00–17:00 EST. Correlation coefficients (r^2) and slopes of the regression lines are given in the upper right-hand corners in colors corresponding to the appropriate model scenario.

ACPD
12, 12801–12852, 2012

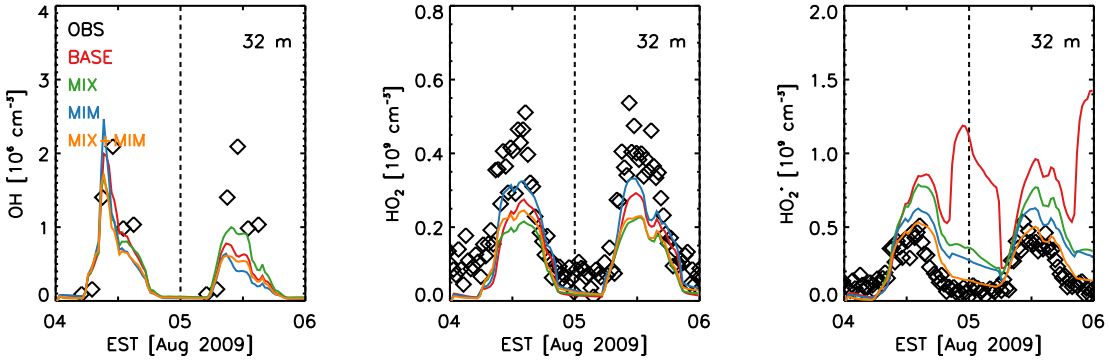

Fig. 8. Same as Fig. 3, but for OH (left), HO_2 (middle), and HO_2^* (right) at 32 m.

ACPD
12, 12801–12852, 2012

Modeling in-canopy chemistry during CABINEX 2009

A. M. Bryan et al.

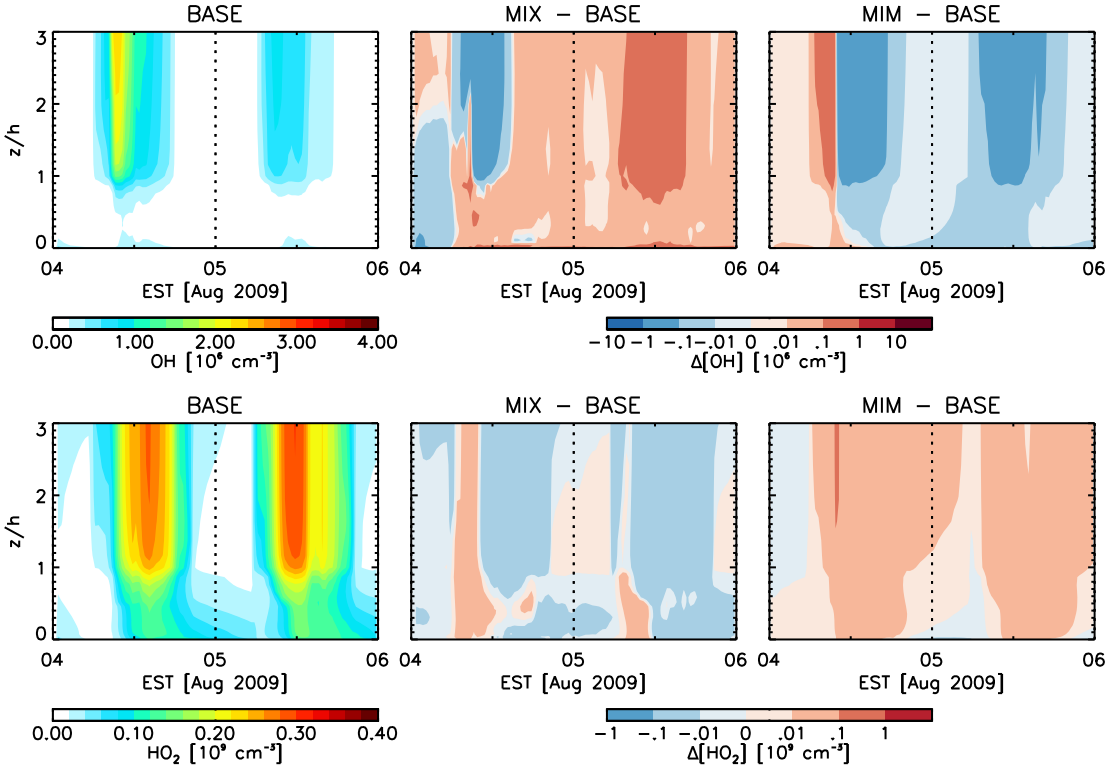

Fig. 9. Vertical profiles of modeled OH (top) and HO_2 (bottom) for the BASE case (left) and the absolute difference between the BASE and MIX cases (middle) and BASE and MIM cases (right). Blue values indicate higher concentrations in the BASE case, and red values indicate higher concentrations in the MIX or MIM cases.

ACPD
12, 12801–12852, 2012

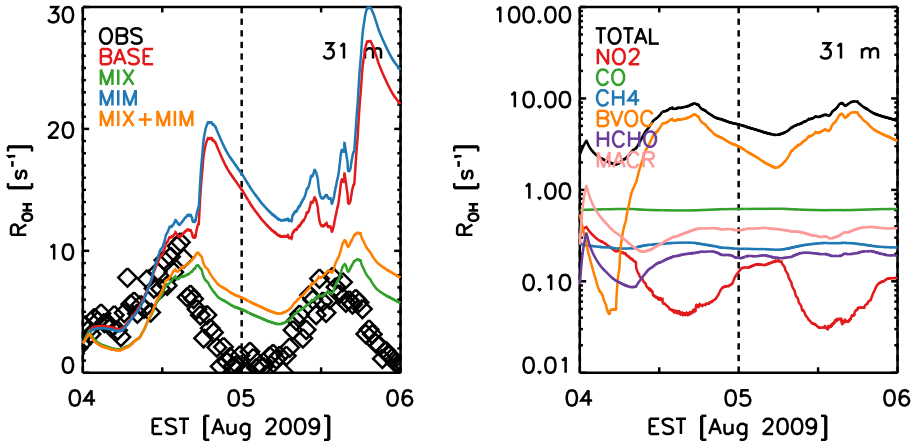

Fig. 10. Total OH reactivity measured (OBS) and modeled (BASE, MIX, MIM, and MIX+MIM) at 30.9 m for 4–5 August 2009 (left); modeled total OH reactivity and from speciated contributions of NO_2, CO, CH_4, BVOC (ISO + API + LIM), HCHO, and MACR for the MIX case (right).

ACPD
12, 12801–12852, 2012